THE UNIVERSITY OF OKLAHOMA

GRADUATE COLLEGE

EFFECTS OF LARGE-SCALE SUBSIDENCE ON CELLULAR CONVECTION IN THE ATMOSPHERE: A NUMERICAL EXPERIMENT

A DISSERTATION

SUBMITTED TO THE GRADUATE FACULTY

in partial fulfillment of the requirements for the

degree of

DOCTOR OF PHILOSOPHY

BY

STANLEY LOUIS BARNES

Norman, Oklahoma

1967

EFFECTS OF LARGE-SCALE SUBSIDENCE ON CELLULAR

CONVECTION IN THE ATMOSPHERE:

A NUMERICAL EXPERIMENT

APPROVED BY

DISSERTATION COMMITTEE

ACKNOWLEDGEMENTS

The author's deepest gratitude is extended to Prof. Y. Sasaki whose concern, timely guidance, and encouragement were paramount contributions to the accomplishment of this research. Appreciation is also extended to Mrs. Kathryn Brigham for her assistance in typing the paper.

This research was performed under the sponsorship of the Environmental Science Services Administration, Grant WBG-57 awarded to the University of Oklahoma Research Institute and was in connection with graduate study at the University of Oklahoma.

TABLE OF CONTENTS

LIST OF TABLES

LIST OF ILLUSTRATIONS

Illustration | Page

EFFECTS OF LARGE-SCALE SUBSIDENCE ON CELLULAR CONVECTION IN THE ATMOSPHERE: A NUMERICAL EXPERIMENT

CHAPTER I

INTRODUCTION

The cellular nature of convective systems has been observed for many decades. Stratified fluids which attain a degree of bouyancy through heating of their lower layers, or cooling their upper layers, will initiate circulation modes in which warmer portions of the fluid rise and cooler portions descend. This convective motion takes place with varying degrees of organization. Under certain conditions, depending on the molecular properties of the fluid, the temperature excess at the bottom, and the depth of the fluid, the convection organizes into a distinct cellular pattern with regions of updraft and downdraft which are essentially laminar flow (Rayleigh, 1916). Under other conditions, if the heating occurs too rapidly or the molecular viscosity and conductivity are small, a turbulent regime of bouyant elements is manifested with no organization to the flow, at least on the scale which we can observe. In general, the atmosphere exhibits both turbulent and laminar convection superimposed in varying degrees (Sutton, 1953). It is the organized cellular convection which is of primary concern in this paper.

Because motions in the atmosphere can be organized on an extremely wide range of scale lengths, the patterns observed are indeed varied (see, for example, Ludlam and Scorer, 1953). They range in appearance from singular bubbles (cumulus clouds) to jet-like plumes (smoke-stack effluents) to honeycombed cells (altocumulus clouds). On a larger scale, the thunderstorm cloud (cumulonimbus) exhibits both bubble-like (Scorer and Ludlam, 1953) and plume-like (Squires and Turner, 1962) characteristics. Even larger are the traveling cyclones of the mid-latitudes which have an organized pattern of weak up-and down-motions that are not the direct result of localized heating as in simple cellular convective patterns. They are more associated with latitudinal temperature gradients and are typified by horizontal convection in which the earth's rotation plays a large role (see, for example, Haltiner and Martin, 1957).

During the past seven years, numerous examples of the honeycomb cell pattern have been observed in meteorological satellite photographic data on a scale theretofore not anticipated. Prior to that discovery (Krueger and Fritz, 1961), cellular convective patterns in which the up and down motions took on the form of polygons had been observed only in the laboratory (Bénard, 1901; Avsec, 1939) and in certain forms of limited convective cloud layers such as altocumulus, stratocumulus, and cirrocumulus. The cellular patterns in those cloud forms are often associated with strong radiative cooling.

The experimental work by Bénard and the theoretical approach by Rayleigh and numerous later investigators revealed the cells to be of a height-width ratio of order one. In the atmosphere, such a ratio is approximated only on the scale of the individual elements in the cloud layers mentioned previously. The cellular cloud patterns observed by satellites occur in a layer 1 to 2 km deep and are from 10 to 100 km across, giving a height-width ratio of order 1/10 to 1/100 (Fig. 1).

The reasons for that ratio are not yet completely understood. In most other descriptive aspects, the atmospheric cells are similar to those of the laboratory models and of the theoretical investigations. When the fluid is heated slowly from below, convective currents begin to rise through a neutrally stable environment and finally reach an upper boundary (a conducting rigid surface in laboratory experiments; a temperature inversion in the atmosphere). Because the system is closed, return circulations develop under the conditions of mass continuity. (Laboratory fluids and the atmosphere may be considered incompressible in these cases.) The effect of rotation about the vertical axis (Coriolis in the atmosphere) is to elongate the cell in the vertical (Chandrasekhar, 1953; Chandrasekhar and Elbert, 1955).

Only recently have any realistic results been obtained showing a favorable flattening of the cells in the horizontal direction. Ray and

Scorer (1963) were able to obtain flat cells by assuming a variation of eddy viscosity and conductivity in space. Sasaki (1965) explained the flattening of such cells by considering a mathematical model in which the upward turbulent transports of heat and momentum from the surface boundary layer play an important role. Between the surface boundary layer and a stable layer which limits the upward turbulent transports, a fully-turbulent region was assumed to exist. The resulting factors which he found to govern the wave length of maximum amplification of disturbances in the fully-turbulent layer were the rate of upward heat flux from the surface boundary layer, the depth and eddy coefficients of the turbulent layer, and the static stability in the upper boundary layer. For reasonable values of those parameters associated with cellular cloud patterns, the wave length most amplified was of order 10 km. In an independent numerical convection model, Lugt and Schwiderski (1966) also found that the characteristic wave length is dependent upon the intensity of the heat source.

In this paper we shall begin with the hypothesis that a flattened cellular convective pattern exists in the atmosphere on the scale observed in satellite photographs. As in Sasaki's treatment, we shall imply the layer below the capping temperature inversion to be fully turbulent, supplying heat to the base of the inversion at a rather steady rate by the process of turbulent conduction. The region of interest will be the inversion layer itself. With an assumed periodic variation in the horizontal temperature distribution throughout the inversion, we shall then observe the flow by a numerical solution of the governing equations. The influence of a larger-scale downward motion (subsidence) upon that flow is to be investigated. The model also includes the effect of Coriolis, of radiation, and of turbulent transports of heat and momentum.

CHAPTER II

THE GOVERNING EQUATIONS

The set of equations which govern this convective model is comprised of the Navier-Stokes equations of motion written in a Cartesian (x, y, z, t) system, the equation of mass continuity under the Boussinesq approximation (variations in density are neglected except as they modify gravity to produce bouyancy), and the first law of thermodynamics written for a diabatic process but neglecting contributions due to phase changes of water substance. Molecular viscosity and thermometric conductivity are neglected in comparison to their eddy counterparts which are also considered constant in space and time.

The Perturbation Equations

The equations are linearized in regard to small perturbations from the basic state. Normally, this would allow analytic solutions of the set under an appropriate set of boundary conditions. However, because the basic-state temperature is a function of height, one of the coefficients in the thermodynamic equation is not constant. Although approximate analytical solutions could be obtained in thin layers for which the change of basic-state temperature is considered constant with height, it was felt that a more straight-forward solution by finite-difference techniques would yield more information, particularly in view of the unknown relationships between the other coefficients of the terms in the equations.

The governing equations are derived in Appendix A using a scale analysis similar to that developed by Ogura and Phillips (1962). The equations are in ~~non~~-dimensional form with the notations as defined in Table 1. Under the basic-state conditions $\bar{u} = \bar{v} = 0$, $\bar{w}$ = constant, $\bar{\theta} = \bar{\theta}(z)$, and neglecting variations in the y-direction, the following equations are obtained.

$$\frac{\partial u'}{\partial t} = -\bar{w}\frac{\partial u'}{\partial z} - \frac{\partial \pi'}{\partial x} + \alpha v' + K_x \frac{\partial^2 u'}{\partial x^2} + K_z \frac{\partial^2 u'}{\partial z^2}, \tag{1}$$

$$\frac{\partial v'}{\partial t} = -\bar{w}\frac{\partial v'}{\partial z} - \alpha u' + K_x \frac{\partial^2 v'}{\partial x^2} + K_z \frac{\partial^2 v'}{\partial z^2}, \tag{2}$$

$$\frac{\partial w'}{\partial t} = -\bar{w}\frac{\partial w'}{\partial z} - \frac{\partial \pi'}{\partial z} + \theta' + K_x \frac{\partial^2 w'}{\partial x^2} + K_z \frac{\partial^2 w'}{\partial z^2}, \tag{3}$$

$$\frac{\partial u'}{\partial x} + \frac{\partial w'}{\partial z} = 0, \tag{4}$$

$$\frac{\partial \theta'}{\partial t} = -\bar{w}\frac{\partial \theta'}{\partial z} - w'\frac{\partial \bar{\theta}}{\partial z} - A\theta' + K_x \frac{\partial^2 \theta'}{\partial x^2} + K_z \frac{\partial^2 \theta'}{\partial z^2}. \tag{5}$$

The primes represent perturbation quantities; the overbars are for basic-state quantities. Non-dimensional Coriolis parameter is represented by α. In (5), $-A\theta'$ is the radiation term represented to the same degree of approximation as the rest of the terms (see Appendix A). $\overline{\theta}$ and θ' are temperature deviations from that of an adiabatic atmosphere.

In set (1) through (5), we have taken eddy viscosity and eddy conductivity to be equal. The validity of that approximation is open to discussion. Sutton (1953) and Priestley (1959) have remarked about the dependency of the vertical heat and momentum eddy coefficients upon the stability of the atmosphere. Experimental results indicate the ratio of the coefficients varies about one in the atmospheric boundary layer, depending upon the Richardson number. More recently, Lilly (1962) obtained numerical results in convective models which suggest that the dependency of eddy viscosity upon the Richardson number is small except in the initial stages of development and in stably-stratified regions. However, lacking any quantitative information from either experiment or theory, we have chosen to equate the processes of eddy heat and eddy momentum exchange.

The reader will note the eddy coefficients have been written in two-component form: K_x the horizontal component, and K_z the vertical component. Priestley (1962) suggests that the two components are unequal under stable stratification and with a ratio on the order of 100, K_x to K_z. We shall make use of that suggestion later. However, the results indicate that ratio is somewhat too small, at least for the convection modeled here.

The Basic State

The atmospheric environment in which flat cellular convection occurs has been observed by Krueger and Fritz to be characterized by a layer some 1 to 2 km deep having a neutral or slightly unstable stratification in the lower portion and capped by a stable layer usually in the form of an inversion of temperature. The layer is heated from below and has little vertical shear of the wind throughout. The temperature inversion is generally thought to be of the subsidence type. That is, weak uniform downward motion maintains the inversion by adiabatic warming against the destructive effects of eddy conduction and radiation. Although there are no direct measurements of vertical motions on the scale of concern (greater than 100 to 200 km), the subsidence is implied because of the somewhat persistent nature of such inversions.

The basic state of the stable layer is, therefore, regarded as having no horizontal motion, weak but uniform downward motion, and a temperature distribution which is steady, resulting from a balance between adiabatic warming and vertical eddy conduction. (The radiative effects turn out to be negligible when considering the conditions applicable to the present model. The conditions under which radiation would become important, that is, the presence of a thick cloud layer or an extremely sharp inversion (Möller, 1951), are not relevant to the model.)

Since we are making the simplification that the eddy coefficients are constants, the vertical basic temperature profile must therefore be such that the magnitude of its curvature is sufficient to balance the warming effect of subsidence. The equation governing the basic-state temperature profile is derived in Appendix B. The result is noted here.

$$\overline{\theta} = \overline{\theta}_o \left[\frac{\exp(\overline{w}/K_z)z - \exp(\overline{w}/K_z)}{1 - \exp(\overline{w}/K_z)} \right] , \qquad 0 \leqq z \leqq 1. \tag{6}$$

Thus, the overall stability within the layer depends upon the choices of $\overline{w}$ and K_z. Once specified, relationship (6) will assure that the curvature of the profile is sufficient to maintain the steady condition. In this regard, we must be guided in our choices of $\overline{w}$ and K_z so as not to require too much of the curvature. As the ratio $\overline{w}/K_z$ increases, the profile approaches that of an infinitesimally thin temperature inversion. While such layers are sometimes observed in the atmosphere (particularly in <u>strong</u> subsidence regions), it is the purpose of this investigation to study the details of the flow <u>in</u> the inversion. We must therefore chose $\overline{w}/K_z$ so that the portion of the model layer which has an inverted temperature lapse is sufficiently thick. The actual values chosen will be discussed in Chapter IV.

Reformulation of the Perturbation Equations

It is common in numerical models of this nature to simplify the governing equations by eliminating the perturbation pressure from the equations. This is accomplished by cross-differentiating (1) and (3), then subtracting to form the vorticity equation:

$$\frac{\partial\eta'}{\partial t} = -\bar{w}\frac{\partial\eta'}{\partial z} - a\frac{\partial v'}{\partial z} + \frac{\partial\theta'}{\partial x} + K_x\frac{\partial^2\eta'}{\partial x^2} + K_z\frac{\partial^2\eta'}{\partial z^2}. \qquad (7)$$

In this case, the vorticity is about a horizontal axis normal to the x-z plane and is defined by the expression

$$\eta' = \frac{\partial w'}{\partial x} - \frac{\partial u'}{\partial z}. \qquad (8)$$

Further, since the flow is essentially incompressible, we may define a streamfunction such that

$$u' = -\frac{\partial\psi'}{\partial z}, \qquad w' = \frac{\partial\psi'}{\partial x}, \qquad (9)$$

and

$$\eta' = \nabla^2\psi' \qquad (10)$$

where the Laplacian is two-dimensional in x and z.

Now, since the perturbations with which we are concerned are periodic in horizontal space (see Fig. 1), we shall assume a convenient form for the dependent variables:

$$\begin{aligned} u' &= U(z,t)\sin kx; & \theta' &= -T(z,t)\cos kx; \\ v' &= -V(z,t)\sin kx; & \eta' &= H(z,t)\sin kx; \\ w' &= -W(z,t)\cos kx; & \pi' &= \Pi(z,t)\cos kx; \\ & & \psi' = -\psi(z,t)\sin kx. \end{aligned} \qquad (11)$$

Inserting (11) into (7), (2), and (5), we obtain the final form of the governing differential equations:

$$\frac{\partial H}{\partial t} = -\bar{w}\frac{\partial H}{\partial z} + \alpha\frac{\partial V}{\partial z} + kT - k^2K_xH + K_z\frac{\partial^2 H}{\partial z^2}, \tag{12}$$

$$\frac{\partial V}{\partial t} \doteq -\bar{w}\frac{\partial V}{\partial z} + \alpha U - k^2K_xV + K_z\frac{\partial^2 V}{\partial z^2}, \tag{13}$$

$$\frac{\partial T}{\partial t} = -\bar{w}\frac{\partial T}{\partial z} - W\frac{\partial \bar{\theta}}{\partial z} - AT - k^2K_xT + K_z\frac{\partial^2 T}{\partial z^2}. \tag{14}$$

Vorticity equation (10) takes the form

$$H = k^2\psi - \frac{\partial^2\psi}{\partial z^2}. \tag{15}$$

From a given set of initial conditions, we may compute new values of H, V, and T using (12) through (14). Eq. (15) is then solved under suitable boundary conditions to obtain a field of ψ which determines U and W by the following relationships:

$$U = \frac{\partial\psi}{\partial z}, \tag{16}$$

$$W = k\psi. \tag{17}$$

The process is repeated for the next time step, and so on until the termination of the calculation.

CHAPTER III

THE NUMERICAL MODEL

Equations (12) through (17) of Chapter II are applied to study the effects of large-scale uniform subsidence upon cellular convection which occurs in a stably-stratified layer to which heat is continually added from the bottom by turbulent conduction. The depth of the stable layer is taken to be 1 km. The layer is equally divided into forty sub-layers by a system of forty-one grid points at 25-m intervals.

The governing equations are approximated in finite-difference form using forward time differences and centered space differences to evaluate the derivatives (except at the upper and lower boundary points where uncentered space differences are used).

The Finite-Difference Equations

The forward-time-step method of solution is subject to computational instability if too large a time increment is used in comparison to the space increment and other parameters (Dingle and Young, 1965). In general, specific stability criteria have been developed only for simple differential equations of the parabolic, elliptic, or hyperbolic types.

Therefore, an analysis will be necessary in order to determine the requirements for the stability of the more complicated set of equations used in this model (see Appendix C).

Corresponding to (12), (13), and (14), the finite-difference equations applicable to the m^{th} grid point (exclusive of the boundary points) and to the n^{th} time step are as follows:

$$\begin{aligned} H(m,n+1) = & [\,1 - k^2K_x\Delta t - 2K_z\Delta t/(\Delta z)^2\,]\,H(m,n) \\ & + [\,K_z\Delta t/(\Delta z)^2 - \bar{w}\Delta t/2\Delta z\,]\,H(m+1,n) \\ & + [\,K_z\Delta t/(\Delta z)^2 + \bar{w}\Delta t/2\Delta z\,]\,H(m-1,n) \\ & + \quad k\Delta t\; T(m,n) \\ & + \quad (\alpha\Delta t/2\Delta z)\,[\,V(m+1,n) - V(m-1,n)\,]\;; \end{aligned} \tag{18}$$

$$\begin{aligned} V(m,n+1) = & [\,1 - k^2K_x\Delta t - 2K_z\Delta t/(\Delta z)^2\,]\,V(m,n) \\ & + [\,K_z\Delta t/(\Delta z)^2 - \bar{w}\Delta t/2\Delta z\,]\,V(m+1,n) \\ & + [\,K_z\Delta t/(\Delta z)^2 + \bar{w}\Delta t/2\Delta z\,]\,V(m-1,n) \\ & + \quad \alpha\Delta t\; U(m,n); \end{aligned} \tag{19}$$

$$\begin{aligned} T(m,n+1) = & [\,1 - k^2K_x\Delta t - 2K_z\Delta t/(\Delta z)^2 - A\Delta t\,]\,T(m,n) \\ & + [\,K_z\Delta t/(\Delta z)^2 - \bar{w}\Delta t/2\Delta z\,]\,T(m+1,n) \\ & + [\,K_z\Delta t/(\Delta z)^2 + \bar{w}\Delta t/2\Delta z\,]\,T(m-1,n) \\ & - \quad \beta(m)\Delta t\; W(m,n); \end{aligned} \tag{20}$$

with $m = 2, 3, \ldots, M-1$ and $n = 1, 2, 3, \ldots$. The static stability $\partial\bar{\theta}/\partial z$ is represented by $\beta(m)$ in (20) and is expressed as

$$\beta(m) = \left[\frac{\overline{\theta}_o(\overline{w}/K_z)}{1 - \exp(\overline{w}/K_z)} \right] \exp(\overline{w}(m-1)\Delta z/K_z) \tag{21}$$

with m = 1, 2, 3, . . . , M. It will be noted that the coefficients in (18), (19), and (20) have been chosen arbitrarily constant except for $\beta(m)$ which varies with height. Since those equations are all of the same form and since the temperature perturbation is the driving force for the model, we shall limit our discussion of the computational stability to (20). That discussion is found in Appendix C.

Completing the set of finite-difference equations, we have a recursion formula for the vorticity equation (15) which requires only knowledge of H(m, n) and boundary values of $\psi(1, n)$ and $\psi(M, n)$.

$$\psi(m, n) = [S(m-1)\ \psi(m+1, n) + R(m)] / S(m) \tag{22}$$

with

$$S(m) = [2 + (k\Delta z)^2]\ S(m-1) - S(m-2)$$

and

$$R(m) = S(m-1)\ H(m, n)\ (\Delta z)^2 + R(m-1)$$

for m = 2, 3, 4, . . . , M-1 and under the conditions S(0) = 0, S(1) = 1, and R(1) = $\psi(1, n)$. Formula (22) is derived in Appendix D.

The solution of (22) for the thirty-nine interior grid points is accomplished by first evaluating S(m) and R(m) with m = 2, 3, 4, . . . , M-1 and then, with the upper boundary value of ψ specified as zero, solving (22) for m = M-1, M-2, . . . , 3, 2. The lower boundary value of ψ is determined from the condition on W (see (24) and the discussion of the boundary conditions in the next section, specifically (27)).

With ψ so determined, we may then calculate (16) and (17) by

$$U(m,n) = [\ \psi(m+1,n) - \psi(m-1,n)]/2\Delta z \tag{23}$$

and

$$W(m,n) = k\,\psi(m,n)\ . \tag{24}$$

Boundary Conditions

The boundary conditions in this model are decidedly different from those usually taken in such studies. In Rayleigh's initial theoretical approach, he confined the convective layer between free, conducting surfaces at the top and bottom. A "free" boundary is one which has zero momentum flux between it and the fluid. Thus, no kinetic energy generated by bouyancy is lost to the boundaries. Free boundary conditions have been criticized by Jeffreys (1926) and by Pellew and Southwell (1940) as being unrealistic (except in the atmosphere) and not applicable for laboratory experimentation. Those investigators have required at least one of the horizontal boundaries to be rigid and have found the critical Rayleigh number to be a function of the boundary conditions. More recently, Deardorff (1964) finds that the free boundary condition produces considerably more upward heat flux than is obtainable in laboratory models for which the boundary conditions are rigid. While the rigid condition is adequate for the analytical study of laboratory models, it is not applicable to both boundaries in the meteorological problem, particularly to the problem confronted in this paper.

Because we intend to study the flow in the stable layer which caps the turbulent region below, we are not at liberty to close the lower boundary, for it is through that boundary that the turbulent energy which drives the cellular motions must enter. On the other hand, since the top of the model is several hundred meters above the temperature inversion, it was felt that a significant portion of the convective energy would not reach that boundary. A rigid top boundary was chosen with $U = V = W = 0$ at that level. As the results later indicate, however, a free upper boundary condition probably should have been chosen.

In addition to the kinematic boundary conditions, some constraints upon temperature must be specified. Generally speaking, we may choose the boundaries to be either conducting or insulating. Only the former is applicable to the study of quasi-steady convection cells, for as Pellew and Southwell point out, ". . . unless the temperature at each surface is kept constant at some cost in heat transmission, any instability discovered in analysis must relate to some temporary distribution of temperature, and will be succeeded by some motion having (ultimately) the nature of a damped oscillation . . . ." Thus, we shall assume in the model that the temperature perturbation is zero at the upper boundary and positive constant at the lower boundary for all time.

Because we have relaxed the constraint on W at the lower boundary in an attempt to approximate a physically real model, we must now impose further constraint on the temperature distribution, $T(z,t)$. Upon setting the left-hand side of (14) equal zero for the lower boundary condition on T, we are left with the necessity of balancing the remaining terms of the equation. In other words, the temperature changes by advection from both the basic and perturbation vertical velocities, the horizontal and vertical eddy conductions and the radiative changes must all cancel.

Since the layer is warmer at the bottom than at the top, $\partial T/\partial z$ will necessarily be negative at the lower boundary. Combined with a subsiding basic flow ($\overline{w} < 0$), the advective heat change due to the first term on the right of (14) is a cooling effect. Similarly, with T positive constant at the lower boundary, the horizontal eddy diffusion and the radiation term (third and fourth terms) contribute to cooling. The only terms in (14) which may contribute to warming at the lower boundary are the advective change due to perturbation motion (second term) and the vertical eddy conduction by virtue of a positive curvature of the T-profile (fifth term). We are tacitly assuming that K_x and K_z can never be negative. Since we do not wish to restrict the sign of W to be only negative at the outset, we must determine an initial T-distribution which allows sufficient warming to take place to counter the cooling effects mentioned above. Thus, there must exist initially a divergence of heat flux of the negative sense at the lower boundary.

Normally, the heat flux is specified $\partial T/\partial z$ equals a constant at the boundary. (See, for example, Jeffreys, 1926) However, use of such a condition here would yield only $W<0$ at the boundary since the vertical eddy conduction term would drop out. We would then be left with the physically unrealistic result of a warm temperature perturbation producing a negative acceleration.

We may satisfy the upper and lower boundary conditions as well as the constraint discussed above by choosing the following form for initial T:

$$T(z,0) = T_o \exp(-\gamma z); \qquad \gamma>0. \tag{25}$$

Substitution of (25) into (14) while noting that $W(0,0) = 0$ yields a solution for γ:

$$\gamma = [-\overline{w} \pm (\overline{w}^2 + 4K_z(k^2K_x + A))^{1/2}]/2K_z \tag{26}$$

from which we extract the positive root in order to satisfy $\gamma>0$. We may now use (14) and (26) to solve for a boundary value of W at the n^{th} time step.

$$W(1,n) = [(K_z\gamma^2 - k^2K_x - A + \overline{w}/\Delta z)T_o - (\overline{w}/\Delta z)T(2,n)]/\beta(1). \tag{27}$$

Eq. (27) with (24) serves to complete the boundary conditions.

While (27) does not guarantee $W(1,n)>0$ for all time, it will allow upward motion to occur until the cooling effects become larger than the heating due to eddy conduction. That imbalance may occur as a result of the changing T-profile.

Finally, opening the lower boundary introduces a new energy sink not usually found in classical convective models. Non-hydrostatic pressures at the lower boundary may now work against the convective motions in the stable layer.

The Energy Integral

The equations expressing the rate of change of kinetic and available potential energies are obtained from set (1) through (5). By multiplying (1) by u', (2) by v', and (3) by w', then adding, one obtains

$$\begin{aligned}\frac{\partial(KE)}{\partial t} = &- \overline{w}\,\frac{\partial(KE)}{\partial z} - \frac{\partial(u'\pi')}{\partial x} - \frac{\partial(w'\pi')}{\partial z} + \pi'\left(\frac{\partial u'}{\partial x} + \frac{\partial w'}{\partial z}\right) + w'\theta' \\ &+ K_x\left[u'\frac{\partial^2 u'}{\partial x^2} + v'\frac{\partial^2 v'}{\partial x^2} + w'\frac{\partial^2 w'}{\partial x^2}\right] \\ &+ K_z\left[u'\frac{\partial^2 u'}{\partial z^2} + v'\frac{\partial^2 v'}{\partial z^2} + w'\frac{\partial^2 w'}{\partial z^2}\right] \qquad (28)\end{aligned}$$

where $KE = (u'^2 + v'^2 + w'^2)/2$. Note that the fourth term on the right of (28) is zero by virtue of (4), and the kinetic energy of the constant basic flow is not considered. Since the system of equations is linear, there can be no energy exchanges between the perturbation and the basic flows.

Similarly, if we multiply (5) by θ' and divide by β, we obtain an expression for available potential energy:

$$\frac{\partial(PE)}{\partial t} = -\frac{\overline{w}}{2\beta}\frac{\partial\theta'^2}{\partial z} - w'\theta' - \frac{A\theta'^2}{\beta} + K_x\frac{\theta'}{\beta}\frac{\partial^2\theta'}{\partial x^2} + K_z\frac{\theta'}{\beta}\frac{\partial^2\theta'}{\partial z^2} \qquad (29)$$

where PE = $\theta'^2/2\beta$. The available potential energy is dependent only upon the mass distribution or, in the case of an incompressible fluid, the temperature distribution (Lorenz, 1955). Also, available potential energy is always regarded as positive for temperature perturbations of either sign, hence the θ'^2 form.

Although energy is not conserved in this model, it will be useful to look at the energy integral over a suitable volume of the model. Since our model is composed of periodic horizontal variations and is linear, integration over one wave length and then over the depth of the layer is sufficient. (Variations in the y-direction are ignored; integration over a unit distance in y is implied.) Substituting u', v', <u>etc.</u> from (11) into (28) and (29) and carrying out the volume integrations, we have

$$\frac{\partial\overline{\overline{(KE)}}}{\partial t} = \overline{w}(KE)_{z=0} - W(0,n)\,\Pi(0,n) + \overline{\overline{WT}} - 2k^2K_x\overline{\overline{(KE)}}$$

$$+ K_z\overline{\overline{\left[U\frac{\partial^2 U}{\partial z^2} + V\frac{\partial^2 V}{\partial z^2} + W\frac{\partial^2 W}{\partial z^2}\right]}} \qquad (30)$$

and

$$\frac{\partial\overline{\overline{(PE)}}}{\partial t} = -\frac{\overline{w}}{2}\overline{\overline{\left[\frac{1}{\beta}\frac{\partial T^2}{\partial z}\right]}} - \overline{\overline{WT}} - \overline{\overline{\left[\frac{AT^2}{\beta}\right]}}$$

$$- 2k^2K_x\overline{\overline{(PE)}} + K_z\overline{\overline{\left[\frac{T}{\beta}\frac{\partial^2 T}{\partial z^2}\right]}}. \qquad (31)$$

The double bar above a term indicates a vertically-averaged quantity. In (30), kinetic energy is lost due to subsidence ($\overline{w}<0$) advecting it through the lower boundary (first term on the right), due to working against the pressure forces acting along the lower boundary (second term), and due to horizontal turbulent diffusion (fourth term). The vertical diffusion (fifth term) may act as either a source or sink. The principal source of kinetic energy appears in the $\overline{\overline{WT}}$ term which links the changes in kinetic energy to the changes in potential energy in (31). Of course, kinetic energy may also be transformed into potential energy in which case the third term in (30) acts as a sink.

In the potential energy equation (31), we again find sinks due to subsidence (first term), horizontal diffusion (fourth term), and also radiation (third term). The fifth term which is related to the vertical diffusion of potential energy may again be either a source or sink, depending upon the distribution of T in the layer.

The truncation error of the numerical solution of hydrodynamical models is not generally known, *a priori*. The total energy integral is usually a means of estimating the truncation in the finite-difference equations. The total energy integral is the sum of (30) and (31). Although the energy is not conserved in the model, the terms of the total energy integral may be evaluated and, ideally, should sum to zero. Non-zero summation may be taken as a guide to the truncation error. A discussion of the truncation errors is found in Chapter V.

CHAPTER IV

DESIGNATION OF THE EXPERIMENTAL PARAMETERS

For the simplicity of notation and for purposes of comparison in this and the following chapters, we shall refer to the parameters and variables in (18) through (24) by their dimensionless notation (i. e., without asterisks), but when dealing with their numerical values we shall give the dimensional values except where noted. The characteristic time, length and velocity scales are 34.7 sec, 1 km, and 29 m sec^{-1}, respectively.

After the initial choice of the parameters, the only ones which were varied from case to case were horizontal wave number, k, and the basic subsidence flow, $\overline{w}$. Of course, as a result of varying k and $\overline{w}$, the initial temperature distributions varied from case to case and hence the available potential energy. Also, variation of $\overline{w}$ caused a variation in the static stability, β. As a caution against computational instability and truncation error, the time increment was decreased for cases involving shorter horizontal wave lengths. A listing of the constant parameters is found in Table 2, and in Table 3 are found the various cases studied along with the parameters which varied.

Six experiments were run for varying horizontal wave lengths: 1, 5, 10, 20, 50, and 100 km. Then, in an effort to better delineate the effects of subsidence on the convection, the 5-, 10-, 20-, 50-, and 100-km cases were run again with $\overline{w} \sim 0$, making a total of eleven experiments.

The vertical mesh length was 25 m in all cases. The time increment varied from 12 sec for the longer wave lengths to 6 sec for wave lengths 20 km or less, except 2 sec for the 1-km case. The maximum allowable time step depends upon the wave length and varied from about 24 sec to 57 sec based on the analysis of computational stability in Appendix C. The total running time for the experiments varied from 6 hr for wave lengths less than 50 km to 12 hr for the 50- and 100-km cases, with two exceptions. The 20-km subsidence case was run for 12 hr and the 1-km case was run for 4 hr.

Large-scale vertical velocities in the subsidence layers of the lower atmosphere are probably no greater than -10 cm sec^{-1}. Even at that rate, an inversion layer would descend over 1 km in only 3 hr in the absence of any heat sources or sinks. This degree of descent is apparently excessive based on what is observed in soundings of temperature in the atmosphere. Subsidence of 1 km in 24 hr is more nearly what is observed. The value $\overline{w} = -1.5$ cm sec^{-1} is chosen to reflect that magnitude of subsidence.

In the experiments without subsidence, instead of taking $\overline{w}$

literally zero, we assigned a value of $\overline{w} = -1.5 \times 10^{-3}$ cm sec^{-1}. The effect is as though we had retained the radiation term in the exponential governing the basic temperature profile (6). When $\overline{w}$ has a realistically large value, the radiation effect is negligible in determining the basic temperature profile.

Recall, also, that the basic-temperature distribution is maintained by a balance between compressional heating due to subsidence and eddy conduction which cools the layer. In (6), once the ratio $\overline{w}/K_z$ has been established, the balance requirement governs the curvature of the $\overline{\theta}$-profile. To obtain a rather gradual change of $\overline{\theta}$ with height for the benefit of clarifying the results within the temperature inversion and to control truncation errors, we do not wish to require the profile curvature to make up order of magnitude differences in the ratio $\overline{w}/K_z$. In other words, if $\overline{w}/K_z$ is small (much less than 1), the $\overline{\theta}$-distribution approaches that of an isothermal layer (Fig. 2). On the other hand, if $\overline{w}/K_z$ is very large (much greater than 1), the $\overline{\theta}$-distribution approaches that of a zero-order discontinuity. The choice of K_z is limited, then, by the order of the magnitude of $\overline{w}$ and the desire for a gradually changing temperature inversion as a basic state. Since the depth of the model is 10^5 cm, we choose $K_z = 5 \times 10^4$ cm^2 sec^{-1} making the ratio $\overline{w}/K_z = -3$ with $\overline{\theta}$ as shown in Fig. 2.

The chosen value of K_z is only slightly greater than the minimum effective value determined by Ogura (1963) in a numerical experiment on cumulus convection. This is perhaps desirable in view of our incomplete knowledge of the eddy exchange processes on the scale of motion dealt with in the model. We do not wish to overwhelm the rather subtle effects which subsidence may impose upon convective motions. Furthermore, we are somewhat limited in the choice of K_z because of its appearance in the condition for computational stability (see Appendix C). An increase in K_z by an order of ten would require a time step less than 3 sec for the smaller wave lengths. While this is not economically impractical with present generation computers, a larger time step was certainly more desirable.

For a choice of the horizontal eddy coefficient of diffusion, K_x, we must again be guided more by intuition than by knowledge of the fundamental physics of the process. Many investigators have taken K_x and K_z to be the same for lack of any better estimate. On the other hand, values as large as 10^{11} cm^2 sec^{-1} have been deduced as applicable in stable layers based on the ability of gravity waves to disperse heat and momentum at speeds on the order of 100 m sec^{-1} (Sasaki, 1964). Simple scale considerations whereby K_x is estimated as proportional to a representative length times a representative velocity yields a K_x of order 10^8 cm^2 sec^{-1} for this model. This latter value is also consistent with Sasaki's estimate (1965) for the fully turbulent region below the stable layer. Priestley (1962) suggests that a ratio K_x/K_z equal to 100 is necessary to produce the horizontal elongation of the cellular cloud patterns through anisotropic turbulent transport. Since that estimate gives the most conservative value for K_x different from K_z, we shall adopt $K_x = 5 \times 10^6\ cm^2\ sec^{-1}$ as the value in our model.

As discussed in Appendix A, the radiation effect which we are modeling is a large-scale effect. That is, it is the result of temperature distributions whose variations occur over a much larger scale than the perturbation scale in the model. While there is possibly an order of magnitude ambiguity in the estimation of the mean free path of radiation, κ, Goody's (1956) value of $2 \times 10^{-2}\ cm^{-1}$ applicable for water vapor at S. T. P. may be considered an absolute maximum for the atmosphere which usually contains only a few parts water vapor in a thousand parts of air. Thus, the largest effect of large-scale radiation on the perturbation temperature field may be estimated as $A = 16\kappa\delta\Theta^3/s = 4 \times 10^{-6}\ sec^{-1}$.

Designation of the other parameters in Table 2 is less uncertain. The Coriolis parameter, α, is known to be of order $10^{-4}\ sec^{-1}$ in all but equatorial latitudes. The deviation of basic-state temperature $\overline{\theta}$ from Θ at the base of the inversion is arbitrary within the limits that $\Delta\theta/\Theta$ is of order 0. 1. Since $\Theta \sim 300K$, our choice of $\overline{\theta}(0) = -10C$ is well within the requirement. The temperature perturbation at the lower boundary is also arbitrary within the above requirement. $T_o = 3C$ is physically realistic to the convection modeled.

CHAPTER V

RESULTS AND DISCUSSION

The Physical Picture

Before viewing the results, let us elaborate the physical picture described by this convective model. Typically, cellular cloud patterns are observed to occur above a heated portion of the earth's surface where there exists a thermal cap or stable layer (temperature inversion) at an altitude of 1 to 2 km. As surface air is warmed it rises in small convective elements through a layer having nearly neutral stratification. Those convective elements have the forms of bubbles, plumes, and columns which, because of the neutral environment, mix that layer thoroughly producing a fully-turbulent regime. On top of that thermally-mixed layer is a stably-stratified layer which prevents the convective elements from penetrating the atmosphere further. (Occasionally, individual elements or groups of elements do penetrate the stable layer if they possess sufficient bouyant energy or if a larger-scale motion temporarily weakens the inversion. These cases are not of direct concern in this study, although they are an important class of convection. We shall confine our discussion to the weaker, more gradual convective warming for which the rigid boundary condition is more applicable.)

On the whole, there is a net transport of heat upward from the earth's surface to the base of the stable layer via the turbulent convective elements. (Turbulent elements are taken to mean those which produce eddy-like exchanges on a scale below the smallest scale describable by the model.) The magnitude and duration of the warming are governed by the surface temperature excess and conditions in the surface boundary layer (the first several hundred meters of air adjacent to the earth's surface). Over land surfaces, this heating normally has diurnal variation, although under some conditions in cold air masses it may continue throughout the night. Over oceans, the heating may continue for periods longer than 24 hr depending only on the sea-air temperature difference. In any case, for the well-developed cellular convection of the type considered here, the heating would continue in a more or less steady manner over a period of at least 6 to 12 hr. In the model, the effect of this steady upward heat flux is approximated by holding the temperature at the lower boundary constant. However, large-scale subsidence through the inversion tends to diminish temperature excesses. Therefore, a divergence of turbulent heat flux at the bottom of the stable layer is necessary to satisfy the boundary condition.

The processes which establish a temperature excess throughout the stable layer are not modeled. Supposedly, the accumulation of heat near the base of the stable layer would gradually spread upward through the layer by processes of eddy exchange and radiation of a more localized type than that which is considered in the model. Probably, as the excess temperature distribution becomes larger, a critical point is reached whereby the eddy effects cannot maintain sufficient heat transport through the layer, and a laminar convective flow will develop in a manner analogous to the classical Rayleigh-type models. The present model is not directly concerned with establishing the parametric relationships governing the onset of the convective flow. Rather we have assumed that the conditions producing such a flow have already been satisfied, and we have undertaken to determine any preference of scale for that flow and the effects of large-scale subsidence.

To accomplish that aim, we begin with an initial excess temperature distribution which is sinusoidal horizontally and diminishing exponentially toward the top of the layer. The development of the convective flow is then "predicted" by a numerical solution of the governing equations. The top of the layer is held rigid and the bottom left open. Both boundaries are conducting.

The Growth of the Convective Cell

The development of a typical convective cell under the influence of subsidence is shown in Fig. 3 which depicts the streamfunction field at hourly intervals for the first six hours over half the 20-km cell. While the stage of growth at any particular time varies with the horizontal scale of the disturbance, the pattern of development is essentially the same for the various wave lengths tested, with the exception of the 1- and 5-km cells.

We see in Fig. 3a that the cell fills the entire depth of the stable layer at the end of the first hour of growth. (The horizontal scale of the figure is 10 km giving a vertical distortion of 20 to 1 in this case.) At the lower boundary, negative vertical motion has developed in response to the boundary condition on T. That was a general result in the cases with subsidence. The weak downward flow at the lower boundary had little apparent effect within the rest of the layer and never involved more than the lower 50 m. Since there is no reason to believe that feature of the flow represents a real atmospheric condition, we shall dispose of it as simply an inconsequential boundary effect.

By the end of the second hour (Fig. 3b), the circulation center descends from about 250 m to around 175 m, and the entire cell flattens. The magnitude of the circulation diminishes also. Still, the single cell fills the entire depth of the layer.

During the third hour, a secondary, reverse circulation cell develops in the upper half of the layer (Fig. 3c). The lower cell sinks further in the layer to about 150 m and begins to intensify again. The intensification of the lower cell continues during the fourth, fifth, and sixth hours (Fig. 3d, e, and f). The upper cell meanwhile decreases intensity at first, then increases.

In general, the development of the convective cells larger than 5 km exhibited this oscillatory growth pattern. While the development of the upper cell is probably due to the influence of the rigid upper boundary, it is nonetheless considered to be a physically realistic phenomenon. In the actual atmosphere, the ultimate upper boundary is essentially the tropopause. Had it been used as the upper boundary, the center of the upper cell likely would have been just displaced to some higher level.

The experiments without subsidence exhibited similar growth patterns except that the magnitudes of the circulations were greater than in the corresponding subsidence cases.

Variations in the Growth Patterns with Horizontal Wave Length

As mentioned in the last section, the growth of convective cells larger than 5 km is similar except for magnitude and growth rate. This is evident in Fig. 4 which shows the variation with time of the maximum W in the lower cell for each case. In Fig. 4a are the cases with subsidence and in Fig. 4b the cases without.

The oscillatory growth pattern is evident in all cases except the two shortest wave lengths. In the 1- and 5-km cells, the vertical motion quickly reaches a maximum and then remains steady. In the 10- and 20-km cells, the vertical velocities are still increasing at the end of six hours and even at the end of twelve hours in the 20-km non-subsidence case shown in Fig. 4b.

The vertical motions in the 50- and 100-km cells reach an early maximum and slowly diminish in an oscillatory mode. The differences in magnitudes of the vertical velocities between the subsidence and non-subsidence cases can be attributed to two factors. The initial potential energy is greater in each of the non-subsidence cases (see Fig. 5), and the basic-state static stability in those cases is much less in the lower portion of the layer (see Fig. 2). The non-subsidence basic state is nearly isothermal while a temperature inversion of nearly 3.5C in 500 m occurs with the subsidence case.

The amplification preference for the wave lengths 10 to 20 km is even more graphically demonstrated when viewed as the rate of increase of total energy. Because the initial available potential energy varied from case to case, we have represented in Fig. 6 the growth curves for the ratio of total energy to initial energy. Fig. 6a is for the subsidence cases. In the early stages, the 10-km growth rate exceeds that of any other wave length, although at $t \approx 6$ hr it is beginning to level off. The 20-km curves show a greater amplification at $t \approx 6$ hr than any other wave length. The stability of the growth of the 1- and 5-km cells is quite evident.

The appearance of a preferred scale of amplification was predicted in theoretical approaches by Sasaki (1964 and 1965), In the first paper he found the preferred growth scale to lie between 5 and 400 km. The second paper yielded maximum growth at 10 km increasing to infinity as K_x in the turbulent region below the stable layer was increased to a value of 10^8 cm^2 sec^{-1}.

That we have obtained an identical scale of preferred wave length but with $K_x = 5 \times 10^6$ cm^2 sec^{-1} may be attributed to any or all of the following: the horizontal eddy conductivity decreases more than an order of ten in passing from the fully turbulent region into the stable layer; or the models are sufficiently different in the amount of heat energy supplied (Sasaki found a dependency of increasing wave length with increasing upward heat flux); or the choice of a small K_x in this model was offset by a larger than normal turbulent heat transport to the lower boundary. Sasaki's latest model neglects the effects of Coriolis and vertical momentum flux. However, it is felt that these factors cannot explain the discrepancy. As we shall point out in later discussion, there is sufficient evidence from the evaluation of the terms of the energy integral to suggest that our choice of K_x was of insufficient magnitude. It is also likely that we have required too large a turbulent heat flux through the lower boundary (the fact that a downward perturbation flow was required to maintain the constant temperature is indicative of that possibility). It would seem, therefore, that the third of the above mentioned alternatives is the most likely reason for the coincidence between our results and Sasaki's.

Another comparison between this and earlier models is in order. Observation and experimentation have shown that when cumulus or other bubble-type convective cells of size 1 to 5 km reach a stable layer, they are quickly damped out. Yet in the present model, those scales of disturbance reach a steady state. The difference is that the cumulus give a transient warming at the base of the stable layer whereas our model is governed by a steady heat source. Thus, the 1- and 5-km scales of convection in this model are more nearly analogous to plume or columnar convection such as the hot gases from a large conflagration at the surface. In still air, such convection rises vertically over the source and mechanical mixing is minimal as it is in our model.

The steadiness of the 1-km cellular flow is evident in Fig. 7a. which shows the streamfunction pattern for the subsidence case. The pattern shown developed after only 10 min and continued unchanged to the end of the run, 4 hr later. A 1-km non-subsidence case was not run because of the extreme steadiness of this result.

The other patterns in Fig. 7 show the circulation cells at $t = 6$ hr for the other wave lengths. As indicated before, all the cases from 10 to 100 km went through similar growth patterns, differing only in magnitude and timing. The 5-km cell in Fig. 7b does not exhibit the oscillatory behavior. It has retained the indicated pattern and magnitude of circulation through the previous 3 hr. The 50-km case in Fig. 7f appears to be less developed at $t = 6$ hr than the other amplifying cases. It is, however, simply passing at that time through a minimum in its oscillatory growth which is comparable to the 20-km case at $t=2$ hr.

Fig. 8a through 8e indicate the t = 6 hr streamfunctions for the cases without subsidence. Comparing these with the subsidence cases in Fig. 7, it appears that the cells are further along in their development. For example, in the 50-km case (Fig. 8d), the reverse cell has appeared in the upper part of the layer, whereas in the subsidence case (Fig. 7e) it has yet to appear. Also, the maximum value of the streamfunction is generally larger in the non-subsidence cases. However, the non-subsidence cases all started with larger initial available potential energies (see Fig. 5). If we look again at the growth rates for total energy in Fig. 6a and 6b, we note that the total energy in the 50-km subsidence case has increased e-fold in 4.5 hr while a corresponding increase in the non-subsidence 50-km case takes over 6 hr. A similar relationship holds for all the other wave lengths. The reason for such behavior becomes apparent when we look at the individual terms in the energy integrals (30) and (31) in Chapter III.

Energy Relationships

For purposes of discussion we shall designate the following notation for the terms on the right of (30) and (31):

$$\mathrm{ADKE} = \overline{w}(\mathrm{KE})_{z=0}; \qquad \mathrm{PRES} = W(0,n)\,\Pi(0,n);$$

$$\mathrm{HDIF} = 2k^2K_x\overline{\overline{(\mathrm{KE}+\mathrm{PE})}}; \quad \mathrm{ADPE} = \frac{\overline{w}}{2}\overline{\overline{\left[\frac{1}{\beta}\frac{\partial T^2}{\partial z}\right]}}; \quad \mathrm{RAD} = \overline{\overline{\left[\frac{AT^2}{\beta}\right]}};$$

$$\mathrm{VDIF} = K_z \overline{\overline{\left[U \frac{\partial^2 U}{\partial z^2} + V \frac{\partial^2 V}{\partial z^2} + W \frac{\partial^2 W}{\partial z^2} + \frac{T}{\beta} \frac{\partial^2 T}{\partial z^2} \right]}} .$$

In Fig. 9 we have separated the total energy changes for the 50-km cases into available potential energy and kinetic energy parts. Again, because the initial energies in the two cases were different, we present the results as fractions of their initial energies. In the kinetic energy curves we again note that the subsidence case has amplified e-fold quicker than the non-subsidence case. We may conclude that the amplification of the total energy (Fig. 6) reflects in the same sense the growth of kinetic energy of the convection. That is to say, by t = 6 hr, the 50-km cell with subsidence has utilized its available potential energy in a more efficient manner. This observation is substantiated in the potential energy curves of Fig. 9. The 50-km subsidence case has experienced less depletion of available potential energy at t = 6 hr than has the non-subsidence case.

The explanation may be found by a closer analysis of the period between t = 2 hr and t = 4 hr in Fig. 9, when the kinetic energy growth rate diminished considerably in the non-subsidence case compared to the subsidence case. Coincidentally, the available potential energy increased during this same period in both cases, although the phasing is slightly different. This would suggest that kinetic energy was being transformed directly into potential energy during this time period.

Indeed, such was the case, as the plot of WT verifies in Fig. 10.

After a 2-hr period during which potential energy was being converted into kinetic, WT changes sign and the energy transformation is reversed in both cases. The outstanding question is why the kinetic energy growth rate dropped off significantly in the non-subsidence case.

The time change in the various terms of the total energy integral are shown in Fig. 11d and 12d for the two 50-km cases. The difference in the kinetic energy behavior cannot be attributed to the sinks ADKE, ADPE, PRES, RAD, or HDIF. All but the last were ineffective in the non-subsidence case, and HDIF was essentially the same in the two cases. The answer must lie within the remaining term in the energy integral, VDIF.

Unfortunately, the computer was not programmed to display separately the vertical diffusion of kinetic and potential energies. However, we can obtain a qualitative appraisal of the two effects by looking at the vertical profiles of U, V, W, and T for the two 50-km cases. Fig. 13 indicates the U and V profiles for t = 3 hr. Except for a small region near the lower boundary on the U-curves, the profiles indicate positive curvature throughout and of similar order of magnitude along both curves. Likewise, the V-curves have similar curvature. Since the positive and negative values of U and V are nearly equally distributed in both cases, it is considered doubtful that these components, averaged vertically, would contribute significantly to the difference in energy changes between the two cases.

The profiles of W and T are found in Fig. 14 and 15 for all cases and at 3-hr intervals. Attention is first directed to the 50-km W-profiles in both Fig. 14 and 15. In both cases the profiles exhibit negative curvature at t = 3 hr, and as W is positive (except for a thin layer near the lower boundary in the subsidence case), the average of this component to the vertical kinetic energy diffusion is definite negative in both cases.

Now consider the vertical potential energy diffusion in the non-subsidence case (Fig. 15). At t = 3 hr, the T-profile has positive curvature throughout and is greatest where T is maximum negative. Thus, averaged vertically, this contribution is most likely a sink for potential energy. A hand calculation based on the output values of T at 25-m increments indicated the diffusion term is only slightly negative in this case.

The T-profile for the subsidence 50-km case (Fig. 14) has a decidedly different shape at t = 3 hr. In the region of negative T, the curvature goes negative in the upper levels which contributes to an increase in potential energy through diffusion. A hand calculation based on the output data shows the vertically-averaged diffusion term is definite positive by a considerable magnitude.

Thus, the marked differences which were noted in the kinetic energy growth rates during the period t = 2 to 4 hr for the 50-km cases probably can be attributed to the different contributions from the vertical diffusion of potential energy which occurred during that time. In the non-subsidence case, the noted increase in available potential energy was obtained by a decrease in the kinetic energy. In the subsidence case, since the averaged vertical diffusion of potential energy was acting as a source at that time, the average available potential energy was able to increase without as much decrease in the average kinetic energy.

The Physical Role of Subsidence in the Growth Process

In view of the results discussed in the last section, we may now attempt to draw conclusions regarding the physical role of subsidence and vertical diffusion of energy in the model.

As the convective motion initially develops from the lower boundary, it rises upward due to its positive bouyancy. Since the environment is stably stratified, the convective motion will eventually reach a level of neutral bouyancy and, because of its momentum, overshoot that level creating a pool of colder air at a higher elevation. In a bubble-type convective situation where the only excess heat in the layer is that initially designated, the cold pool of air would then begin to descend in response to its negative bouyancy. It would eventually overshoot the neutral bouyancy level traveling downward where it would again be warmer than its environment. And so on until the bouyancy of the convective cell was destroyed by turbulent exchanges with its environment. This description is based on the theoretical considerations of the parcel method wherein the frequency of oscillation of the bubble about the neutral-bouyancy level is the Brunt-Väisälä frequency.

In this model, however, heat is continually added at the lower boundary. Thus, the air at higher levels with a deficit temperature (negative bouyancy) cannot sink back to the neutral level because of the rising air coming up from the lower boundary. The only recourse for the cold air "trapped" in the upper levels is to begin a reverse circulation which must be maintained at the expense of the energy in the lower cell. Since no direct interactions between the upper and lower cells are possible in this linearized model, the energy transport must take place through eddy diffusion, mainly that of eddy momentum transport.

After the two cells are well developed, there seems to be no problem in maintaining sufficient eddy momentum transport to drive the upper cell. This is apparent in Fig. 11d and 12d which show VDIF actually becoming a source of total energy after about 9 hr. However, in the early stages of development while the eddy momentum transport is still small, the kinetic energy distribution apparently gets out of balance with the available potential energy distribution and must diminish periodically while the potential energy becomes adjusted. This is the most likely cause of the oscillatory character of the results.

Large-scale subsidence reduces the temperature variance, particularly in the upper levels away from the source of heat. This has two effects on the upper cell. By reducing the amount of negative bouyancy of that air, it diminishes the tendency for the upper cell to form in the first place. Secondly, it concentrates the available potential energy in the lower levels. This allows the eddy heat transport to become large enough to supply the upper cell with potential energy instead of making the eddy momentum transport the major supplier at the expense of the kinetic energy of the lower cell.

Subsidence has yet another effect on the convective system as a whole. Note in Fig. 9 that after about 8 hr the kinetic energy in the non-subsidence case begins to exceed that of the subsidence case. This was a general result for the amplifying wave lengths as a comparison of Fig. 6a with 6b demonstrates. The reason is found in Fig. 11 and 12. In the non-subsidence cases, the only important energy sinks were the horizontal and vertical diffusions. In the subsidence cases, not only was energy removed through the lower boundary by the large-scale vertical motion, but the convective system lost energy by working against the pressure forces along the lower boundary. As time progressed, first the pressure sink and then the advective sink became dominant, creating a somewhat continuous brake on the development.

Thus, subsidence plays a rather incongruous dual role: it aids the early development of the convection only to damp the development at a later time.

The effect of subsidence on the cells less than 10-km wave length appears to be more simple. In both of the 5-km cases the steadiness of the flow after about 3 hr (Fig. 6) is apparently due to the predominant effect of horizontal eddy diffusion (Fig. 11a and 12a). Indeed, in the subsidence case after t = 1 hr when WT goes negative and remains steady (Fig. 16), the circulation is maintained entirely through vertical eddy diffusion (Fig. 11a).

The analysis of the energy transformations in the 20-km cases is similar to that of the 50-km cases, except that WT remains at a greater negative value over a longer period of time (Fig. 17). Since the vertical eddy diffusion of total energy was a net sink in the 20-km cases (Fig. 11c and 12c), we must conclude that the vertical eddy diffusion of available potential energy was a large source in both cases according to the argument developed previously.

Comments on the Eddy Exchange Coefficients

Considering the energy transformations for all the wave lengths tested, it is apparent from Fig. 11 and 12 that the relative importance of horizontal diffusion in the model is scale dependent, being very large for small-scale circulations and negligible for scales of order 100 km. However, this is not necessarily representative of the atmosphere under the conditions described by the model.

We can be fairly certain that the turbulent diffusion of energy in a stably-stratified region is not isotropic. Nor would we expect the energy diffused vertically to be an order of magnitude larger than the horizontal component. The model results seem to indicate that we have chosen K_x too small relative to K_z by at least an order of magnitude. K_z was assigned its value mainly on the basis of empirical considerations. We balanced subsidence heating with eddy cooling in maintaining a constant basic-state temperature. Large-scale subsidence is limited to order 1 cm sec^{-1}. Our choice of K_z produced a temperature profile close to that of a "mean" stable layer rather than an extremely sharp inversion or an isothermal layer. There does not appear to be any justification for choosing a larger K_z, at least in the context of the present model.

It appears we have chosen K_x numerically too small. An increase in K_x from 5×10^6 cm^2 sec^{-1} to 5×10^7 cm^2 sec^{-1} would have made HDIF the predominant sink in all cases and may have stabilized the growth rates of the wave lengths greater than 10 km. Such a result would have been more in line with what one might intuitively deduce as the effect of a substantial stable layer upon weak, mesoscale convective systems. The apparent necessity of the larger magnitude for K_x lends support to the value 10^8 cm^2 sec^{-1} suggested by Sasaki. And if our restriction on K_z has any real physical significance, then it appears that Priestley's ratio of $K_x/K_z = 100$ is too small under these circumstances.

In several previous investigations into the problem of determining why atmospheric cellular convection has a width-height ratio on the order of 10 to 1 or 100 to 1, mention has been made of the differences in horizontal and vertical coefficients of eddy exchange (Priestley, 1962; Ray and Scorer, 1963). The latter authors treated the eddy conduction coefficient as a function of temperature which varied horizontally. They also considered the horizontal eddy exchange of momentum to be negligible in cellular patterns, and obtained results from a classical-type model which indicated a flattening of the convective cell. While we do not intend to present here a discussion of their approach, we are able to demonstrate how subsidence may enhance the flattening of the cells through its effect on the horizontal momentum exchanges.

In a simple dimensional approach to the exchange coefficients, they are usually equated to the product of a characteristic length times a characteristic velocity. Thus, for example,

$$K_z = W_{max} \, d \tag{32}$$

in our model. Our comparison here will apply to characteristic lengths which are the same, case by case, so we shall ignore the length and regard the exchange coefficients to be proportional to the velocities. Also, we shall consider a two-dimensional horizontal coefficient, K. In view of the above, we have

$$\frac{K}{K_z} \propto \frac{(U_{max}^2 + V_{max}^2)^{1/2}}{|W_{max}|} \tag{33}$$

as a measure of the ratio of horizontal to vertical eddy exchange coefficients. We have calculated ratio (33) for the various cases discussed in the model and compared the subsidence cases with the non-subsidence cases. The result is shown in Fig. 18. Subsidence effectively flattens the kinetic energy distribution in the convective cells. However, the distribution of kinetic energy is only about 20 per cent flatter in the subsidence cases. Therefore, subsidence alone cannot account for the flattened appearance of the atmospheric convective cells, but it is probably a contributing factor of significant value.

No attempt has been made here to use (33) as a definition of the ratio K/K_z. Such simple relationships have little general application to the atmosphere. In fact, it is easy to demonstrate that the mixing-length hypothesis is of little use in defining the eddy exchange processes in a model even as simple as this linearized one.

Deardorff (1966) has approached the problem of explaining counter-gradient heat fluxes in the atmosphere on the basis of a thermal variance equation which is similar to (31), but which includes nonlinear effects. While our results do not bear directly upon Deardorff's analysis, we are in a position to comment upon the generality of his definition of a modified coefficient of eddy conduction:

$$K'_H = -\overline{WT}/(\partial\overline{\theta}/\partial z - \Gamma_c) \qquad (34)$$

where

$$\Gamma_c = (\partial\overline{\theta}/\partial z)_{\text{upper limit}} = \frac{-\frac{\partial}{\partial z}\left(\frac{\overline{WT}^2}{2}\right)}{\overline{WT}}. \tag{35}$$

The single overbar denotes here a horizontally-averaged value. Of course, horizontally-averaged $\overline{\theta}$ is the same as our basic-state temperature.

From the mixing-length hypothesis, the usual definition of K_H is

$$K_H = -\overline{WT}/(\partial\overline{\theta}/\partial z) \tag{36}$$

which has no meaning if $\overline{WT}$ and $\partial\overline{\theta}/\partial z$ are of the same sign. Hence the definition (34). In this model, $\partial\overline{\theta}/\partial z$ is always positive and $\overline{WT}$ may take on either positive or negative values. For example, note the distribution of $\overline{WT}$ in Fig. 14 for the 20-km subsidence case at $t = 6$ hr. The mixing-length definition (36) is obviously insufficient if we require K_H to be positive.

Now let us consider Deardorff's definition (34) which we are admittedly applying outside the context of his analysis just to see how general the relationship might be. We calculated the parameter $\overline{WT}^2$ for the 20-km subsidence case and obtained the distribution shown in Fig. 19. Above $z = 0.5$ km, $\partial(\overline{WT}^2/2)/\partial z < 0$. Although $\overline{WT}$ is only small positive in that region, it is apparent that Γ_c will be much less than $\partial\overline{\theta}/\partial z$ (about 3C km^{-1}), and K_H' is in danger of evaluating negative.

On the other hand, our evaluation of Γ_c is obtained from distributions of W and T which do not include the effect of eddy transport of heat by the eddies themselves. (the nonlinear or triple-correlation terms in the temperature variance equation). Clearly, a more elaborate nonlinear model should be investigated before drawing any conclusions as to the quantitative accuracy of (34). However, on the basis of the results at hand, we suspect that (34) will not prove to be a general relationship.

The Pressure, Advective, and Radiative Sinks

The work done by the convective cell against the pressure forces at the lower boundary is a continual sink of energy for all wave lengths, but it is larger for the longer wave lengths (Fig. 11). Likewise, the advective transports of kinetic and potential energies through the lower boundary by $\overline{w}$ are also sinks. Naturally those sinks are absent in the non-subsidence cases (Fig. 12).

Fig. 11 and 12 also indicate the negligible role which large-scale radiative effects have on this type of convection. Even with an increase in the order of magnitude of A (equivalent to 25C cooling per day), RAD would have a significant effect only on the 50- and 100-km cells.

Truncation Errors

In regard to the use of the total energy integral as a guide for estimating the truncation error involved in the differencing scheme, it failed. The changes in kinetic and potential energies were calculated, added to the sources and sinks, and equated to a residual called the "truncation error." The magnitude of the "error" was found to be as large as some of the source-sink terms. Yet, the smoothness of the numerical results suggests a very small truncation error.

The causes of the large residuals are obscure, although two are suggestive. The finite-difference form of (30) and (31) summed was used to calculate the "error." The energy integral formed from the finite-difference set (18) through (24) would perhaps have been more appropriate. Deardorff (1964) notes a similar problem with the finite-difference formulation of the energy integral.

Also, application of the lower boundary condition (T = constant) to (31) does not produce a constant available potential energy at the boundary. Since no direct use was made of the energy integrals in the time solutions of the governing set, this fact does not affect the results obtained, but it does influence the residual to the total energy integral.

If we assume the real truncation error is some smaller part of the calculated residual, we may consider our results valid provided the cumulative residual (error) does not approach the magnitude of the total energy in the system at any given time. Fig. 20 shows the cumulative error expressed as a fraction of the total energy for the subsidence cases. At $t = 6$ hr, the influence of the cumulative errors appears to be leveling off at a value less than 0.1 Since the governing set of equations allows a maximum perturbation (real plus error) of 10 per cent ($\Delta\theta/\Theta$~0. 1), it is apparent that we have not exceeded the limits of usefulness of the numerical model. Similar cumulative errors were obtained in the non-subsidence cases.

Influence of Coriolis

The Coriolis effect is the primary source of v-motion in (2), whereas u-motion (1) is driven by both pressure gradient and Coriolis forces. An indication of the effectiveness of Coriolis in the cellular convective motions modeled is presented in Fig. 21 which shows the ratio $|v_{max}|/|u_{max}|$ at t = 6 hr for the various wave lengths.

The results are similar in both the subsidence and non-subsidence cases. For wave lengths 5 km and less, the earth's rotation has negligible effect on the convective motions and may justifiably be omitted from the equations. For wave lengths 20 km and greater, however, the motions produced by Coriolis are at least as large as those produced by pressure forces. It is apparent that any study of the horizontal flow in mesoscale disturbances should include the Coriolis effect.

The falling off of the profiles in Fig. 21 between 50 to 100 km is apparently the result of the oscillatory growth behavior of the cells. A check of the ratio for 100 km at t = 12 hr yields values of 3. 50 in the subsidence case and 6. 35 in the non-subsidence case.

Contribution of Subsidence to the Cellular Cloud Patterns

A principal characteristic of the cellular cloud patterns shown in Fig. 1 is their periodicity in space. The periodic nature on the scale ten to a few hundred kilometers has been explained at least partially by Sasaki as a natural consequence of the turbulent structure and upward heat flux found in the atmosphere between the earth's surface and the base of the stable layer capping the convective motions.

Also note in Fig. 1, the variation in the ratio of cloudy to clear air[1] in the overall pattern. The smaller the scale of the convective cells, the more nearly the ratio of cloudy to clear air is equal to one. Some of the larger-scale convective cells generally have much greater clear area than cloudy. These are the "hollow" or "doughnut" cloud patterns first reported by Krueger and Fritz.

Fig. 22 shows how the model results may account for such a distribution. In that figure we have presented one and one-half cycles of the assumed x-variation in w' (returning to our original notation) for typical results in the 50-100 km and 10-20 km scales. Superposed, $\bar{w}$ is represented for the subsidence case, and the ordinate is labeled for the net or total vertical motion $w = \bar{w} + w'$ in cm sec^{-1}. If we

---

[1]The dark portions of the satellite photographs are taken to be clear skies. However, scattered cloud elements too small to be resolved by the camera may be present there.

equate $w > 0$ as indicative of a cloudy region and $w < 0$ for a clear region, we see on the 50-100 km scale (which exhibits relatively small values of w') that the ratio of cloudy to clear is significantly less than one.

On the 10-20 km scale (for which w' reaches much higher values than on the larger scale), the ratio of cloudy to clear is very nearly one. Of course, the magnitude of subsidence varies in space and time, but the effect is notably the same sense as indicated. The smaller, more vigorous cells will have a larger cloudy to clear ratio than the larger cells which have weaker perturbation vertical velocities. The non-subsidence cases would show a cloudy to clear ratio nearly equal to one <u>for any scale.</u>

Naturally, the spatially periodic variations of temperature which are associated with such cellular patterns in the atmosphere are not pure harmonics which probably accounts in some part for the wide variety of cell sizes seen in Fig. 1. This idea is similar to that of Frenzen (1962) who views the cellular cloud pattern as the result of a kind of "beat-frequency" mechanism caused by interactions between the various scales of motion.

Some of the cellular patterns in Fig. 1 exhibit a more cloudy or solid cell center. It is tempting to speculate whether or not this is simply the mirror image of the case shown in the upper part of Fig. 21 with $\overline{w} > 0$. Although the results of his synoptic data studies were somewhat inconclusive, Mitchell (1967) found some cases of these solid, cloud-filled cells associated with apparent, larger-scale upward motion.

The aspects of cellular convection in a field of large-scale slow ascent is an entirely different modeling problem, necessarily nonlinear in nature. There is no physical mechanism for maintaining a steady basic-temperature distribution in an ascending stable layer. In addition, it then becomes necessary to include in some manner the release of latent heat energy, not only in the perturbation but also in the basic flow. In view of the complexities of a "basic ascent flow" model, we can do little more than speculate on the solid-center cellular patterns.

CHAPTER VI

CONCLUSIONS

The numerical model developed in this investigation has dealt with the rather weak, thermal convection associated with cellular (honeycombed) cloud patterns observed by meteorological satellites. Those cloud patterns are typically driven by surface heating and capped by a stable layer of air some 1 to 2 km above the surface. If convective heat transport is large enough or persists for a long period beneath a stable layer, it may eventually destroy the layer and penetrate upward. In order to maintain such a stable layer under such conditions over a period of several hours, a rather gradual, general sinking of the air is required to furnish the necessary heat to offset the eroding effects of the convective elements. The numerical model has been concerned with the effects which general subsidence has on the forced convection entering the base of the stable layer.

For such a study involving slow, rather shallow convection, perturbation solutions of the equations of motion, continuity, and the first law of thermodynamics, modified to eliminate acoustic frequencies, have proven adequate. The formulation of the model differs from previous numerical studies of Rayleigh-type convection in the boundary conditions, in the treatment of the eddy coefficients for heat and momuntum transport, and in the large-scale subsidence of the basic flow. A large-scale radiation factor was also included.

Although the convective cloud elements which make up the observed cellular patterns are governed by the moist-adiabatic process, the larger-scale flow which organizes the cloud pattern is essentially a dry-adiabatic process, especially in view of the subsidence effect. We have, therefore, neglected the contribution of latent heat.

The model was made two-dimensional in x-z space for simplicity only. The effect of the earth's rotation was retained, however, by allowing development of motion perpendicular to the x-z plane.

The upper boundary was rigid and a perfect conductor, although Fig. 13 suggests a free or "slip" condition would have been more appropriate. The lateral boundaries were cyclical, and the lower boundary was open and held at constant temperature, mainly by a balance between advective cooling due to large-scale subsidence and heating due to a divergence of vertical turbulent heat flux. The basic-state temperature was held constant and was stably stratified. The initial temperature excess at the base diminished exponentially with height. Wave lengths of the assumed horizontally-periodic temperature perturbation ranged from 1 to 100 km. Cases with and without subsidence were investigated for comparison purposes.

The significant results were these:

1) The circulation of the growing convective cell first fills the entire layer then forms into two cells, one thermally-driven in the lower part of the layer and the other a reverse circulation which forms in the upper part. The upper cell is driven mainly at the expense of the kinetic energy of the lower cell which transfers upward through the vertical eddy diffusion process (but see paragraph 4 below). The growth process behaves in a damped oscillatory manner, but with the total energy in the system increasing in time (except for the cumulus-scale wave lengths).

2) Convective perturbations of 10 to 20 km horizontal scale were most amplified, with or without subsidence. This supports Sasaki's conclusion (1965) that the scale of the amplified disturbance is mainly a function of the magnitude of heat flux from the surface boundary layer and the horizontal eddy conductivity in the turbulent region below the stable layer.

3) Perturbations less than 10 km were amplified at first, but soon reached a steady state in velocity and temperature distribution. In effect, these waves were damped which is also consistent with earlier investigations.

4) Subsidence aids the development of the growing perturbation in the early stages, but it has an inhibiting effect a few hours later. In regard to the early growth, the vertical diffusion of available potential

energy plays an important role in creating an additional source of energy for the circulation in the upper part of the layer, thus diminishing the necessity for a large eddy transport of kinetic energy vertically.

5) Numerical computation of the relationship between the various sources and sinks in the energy integral indicate that the horizontal exchange coefficient was chosen too small (5×10^6 cm^2 sec^{-1}). It is suggested, though not proven by numerical example, that a value closer to Sasaki's 10^8 cm^2 sec^{-1} applicable for gravitational dispersion of energy in a stable layer would have stabilized the growth rates and perhaps damped the oscillatory growth character of the cells.

6) Subsidence tends to flatten the distribution of kinetic energy in the cells, although it cannot be regarded as the primary cause of the large width to height ratio observed in cellular cloud patterns.

7) The mixing-length definition of eddy conductivity is not valid even for this simplified linear model. Heat flux counter to the gradient of basic-state temperature persisted in portions of the stable layer for every case tested.

8) Large-scale radiation is ineffective as a heat sink over all wave lengths tested.

9) Coriolis is unimportant for horizontal scales much less than 10 km, but becomes significant for disturbances greater than about 20 km for which the motions produced by Coriolis force are at least as large as the motions due to horizontal pressure-gradient force.

10) Subsidence may contribute importantly to the ratio of cloudy to clear air within the observed cellular cloud patterns.

A logical extension of this study is the development of a nonlinear model and further testing of the relationships between horizontal and vertical eddy exchange coefficients. Also, the explicit eddy energy transformations need further clarification which only a nonlinear model can supply. Then, perhaps with a grossly-simplified treatment of the moist-adiabatic process, the model may be applied to the study of the process by which moist convection penetrates a stable layer in an atmosphere which is at rest and in one which has a basic ascent flow.

BIBLIOGRAPHY

Avsec, D., 1939: Thermoconvective eddies in air. Application to meteorology. Air Ministry Works Institute of Fluid Mechanics, Faculty of Sciences, Paris, Sci. and Tech. Publ. No. 155. (Translated from the French by Carl A. Ronne.)

Bénard, H., 1901: Les tourbillons cellulaires das une nappe liquide transportant de la chleur par convection en regime permanent. Ann. d. Chimie et de Physique, **23**, 62-144.

Chandrasekhar, S., 1953: The instability of a layer of fluid heated below and subject to Coriolis forces. Proc. Roy. Soc., A, **217**, 306-327.

Chandrasekhar, S., and D. D. Elbert, 1955: The instability of a layer of fluid heated below and subject to Coriolis forces, II. Proc. Roy. Soc., A, **231**, 198-210.

Deardorff, J. W., 1964: A numerical study of two-dimensional parallel plate convection. J. Atmos. Sci., **21**, 419-438.

________, 1966: The counter-gradient heat flux in the lower atmosphere and in the laboratory. J. Atmos. Sci., **23**, 503-506.

Dingle, A. N., and C. Young, 1965: Computer applications in the atmospheric sciences. Dept of Meteor. and Ocn., College of Engineering, Univ. of Michigan, 256 pp.

Frenzen, P., 1962: On the orgin of certain symmetrical patterns of atmospheric convection. Tellus, **14**, 173-176.

Goody, R. M., 1956: The influence of radiative transfer on cellular convection. J. Fluid Mech., **1**, 424-435.

Haltiner, G. J., and F. L. Martin, 1957: Dynamical and physical meteorology. New York, McGraw-Hill Book Co., 470 pp.

Jeffreys, H., 1926: The stability of a layer of fluid heated below. Phil. Mag., Ser. 7, 2, 834-844.

Krueger, A. F., and S. Fritz, 1961: Cellular cloud patterns revealed by TIROS I. Tellus, 13, 1-7.

Lilly, D. K., 1962: On the numerical simulation of bouyant convection. Tellus, 14, 148-172.

Lorenz, E. N., 1955: Available potential energy and the maintenance of the general circulation. Tellus, 7, 157-167.

Ludlam, F. H., and R. S. Scorer, 1953: Convection in the atmosphere. Quart. J. R. Meteor. Soc., 79, 317-341.

Lugt, H. J., and E. W. Schwiderski, 1966: Convection flows due to local heating of a horizontal surface. J. Atmos. Sci., 23, 54-60.

Mitchell, R. L., 1967: Some considerations of cellular cloud patterns in the atmosphere. Master's Thesis, University of Oklahoma, 58 pp.

Möller, F., 1951: Long-wave radiation. Compendium of Meteorology. Boston, Amer. Meteor. Soc., 34-49.

Ogura, Y., 1963: The evolution of a moist convective element in a shallow, conditionally unstable atmosphere: a numerical calculation. J. Atmos. Sci., 20, 407-424.

Ogura, Y., and N. A. Phillips, 1962: Scale analysis of deep and shallow convection in the atmosphere. J. Atmos. Sci., 19, 173-179.

Pellew, A., and R. V. Southwell, 1940: On maintained convective motion in a fluid heated below. Proc. Roy. Soc., A, 176, 312-343.

Priestley, C. H. B., 1959: Turbulent transfer in the lower atmosphere. Chicago, University of Chicago Press, 130 pp.

__________, 1962: The width-height ratio of large convection cells. Tellus, 14, 123-124.

Ray, D., and R. S. Scorer, 1963: Studies of the problems of cellular convection in the atmosphere. Final Report, U. S. Weather Bureau Contract Cwb-10004, 113 pp.

Rayleigh, O. M., 1916: On convection currents in a horizontal layer of fluid, when the higher temperature is on the under side. Phil. Mag., Ser. 6, 32, 529-546.

Sasaki, Y., 1964: Interaction between small-scale convective and large-scale flow motion. Final Report, U. S. Weather Bureau Contract Cwb-10032, 1-29.

________, 1965: Formation of cellular cloud patterns in the lower atmosphere. Final Report, U. S. Weather Bureau Contract Cwb-10863, 1-18.

Scorer, R. S., and F. H. Ludlam, 1953: Bubble theory of penetrative convection. Quart. J. R. Meteor. Soc., 79, 94-103.

Squires, P., and J. S. Turner, 1962: An entraining jet model for cumulo-nimbus updraughts. Tellus, 14, 422-434.

Sutton, O. G., 1953: Micrometeorology. New York, McGraw-Hill Book Co., 333 pp.

APPENDIX A

DERIVATION OF THE GOVERNING DIFFERENTIAL EQUATIONS

The derivation of the set of differential equations governing this model of a shallow, cellular convective system follows the steps of a scale analysis first performed for atmospheric convection by Ogura and Phillips (1963). The coordinate system is a relative Cartesian system, tangent at the orgin to the earth's surface (i. e., a level surface along which gravity has no component). The positive x-axis is eastward along the local parallel, the positive y-axis is northward along the local meridion, and the positive z-axis is perpendicular to a level surface (along the local plumb line).

For the scale of motions considered in the model (1 to 100 km), the effects of tidal forces and the deviations of the tangent-plane system from a spherical earth are completely negligible (Haltiner and Martin, 1957). Furthermore, we shall neglect molecular viscosity and thermometric conductivity of air in comparison to their eddy counterparts. The former are of order 10^{-1} cm^2 sec^{-1} while the latter are of order 10^4 cm^2 sec^{-1} or larger (Sutton, 1953).

Although the eddy coefficients of viscosity, conductivity, and diffusivity may vary significantly in space and time, there exists little conclusive information, either theoretical or experimental, as to what governs their values. For simplicity, we shall consider the eddy coefficients as absolute constants. However, since the cellular convection to be studied has a characteristic width much greater than its height, we shall consider the horizontal and vertical components of the eddy coefficients to be different in value.

Because the cellular convection which we are studying is essentially symmetrical about the vertical axis, we might have chosen a cylindrical coordinate system. However, we can simplify the equations somewhat by neglecting all variations in the y-direction, thereby making the description of the model two-dimensional without any great loss in generality. We shall, however, retain the Coriolis effect even though the scale of motion is relatively small.

Under the conditions and simplifications stated above, the Navier-Stokes equations of motion are written

$$\frac{du^*}{dt^*} = -\frac{R^*T^*}{p^*}\frac{\partial p^*}{\partial x^*} + f^*v^* + K_x^*\frac{\partial^2 u^*}{\partial x^{*2}} + K_z^*\frac{\partial^2 u^*}{\partial z^{*2}}, \tag{A-1}$$

$$\frac{dv^*}{dt^*} = - f^*u^* + K_x^*\frac{\partial^2 v^*}{\partial x^{*2}} + K_z^*\frac{\partial^2 v^*}{\partial z^{*2}}, \tag{A-2}$$

$$\frac{dw^*}{dt^*} = -\frac{R^*T^*}{p^*}\frac{\partial p^*}{\partial z^*} - g^* + K_x^*\frac{\partial^2 w^*}{\partial x^{*2}} + K_z^*\frac{\partial^2 w^*}{\partial z^{*2}}. \tag{A-3}$$

The equation of mass continuity is expressed

$$-\frac{1}{\rho^*}\frac{d\rho^*}{dt^*} = \frac{\partial u^*}{\partial x^*} + \frac{\partial w^*}{\partial z^*} . \qquad \text{(A-4)}$$

From the first law of thermodynamics with radiation and eddy conduction as sinks or sources,

$$\frac{d\theta^*}{dt^*} = \frac{\Phi^*}{s^*} + K^*_x \frac{\partial^2\theta^*}{\partial x^{*2}} + K^*_z \frac{\partial^2\theta^*}{\partial z^{*2}} \qquad \text{(A-5)}$$

where potential temperature, θ^*, is defined

$$\theta^* = T^*(1000/p^*)^{R^*/c^*_p} ; \qquad \text{(A-6)}$$

p^* being in millibars. A list of symbols used in (A-1) through (A-6) is found in Table 1. The asterisks indicate the parameters have their usual dimensions. The radiation term in (A-5) is expressed in the manner used by Goody (1956):

$$\Phi^* = -\,4\kappa^*\sigma^*T^{*4}. \qquad \text{(A-7)}$$

Relationship (A-7) holds for cases in which the radiation does not vary much over distances comparable to the cell dimensions. By applying (A-7), we are then looking only at the large-scale aspects of the radiation influence. By virtue of this simplification, we cannot expect to learn anything concerning radiative influences within the convective cells themselves.

Equations (A-1) through (A-5) contain solutions expressing the motions for a large spectrum of waves, from very short acoustic waves to ultra-long planetary waves. For the problem at hand, acoustic waves are of no concern and may be considered noise. There are several procedures available for filtering acoustic frequencies from the solutions. One method is performing a scale analysis on the equations. In order to accomplish that, we first write (A-1) through (A-5) in a non-dimensional form using the following definitions:

$$
\begin{aligned}
&\pi = (p^*/P^*)^{R^*/c_p^*}; && T^* = \Theta\pi\theta; \\
&u^* = u(d/\tau); && x^* = xd; \\
&v^* = v(d/\tau); && z^* = zd; \\
&w^* = w(d/\tau); && t^* = t\tau; \\
&K_x^* = K_x(d^2/\tau); && g^* = g(d/\tau^2); \\
&K_z^* = K_z(d^2/\tau); && f^* = a/\tau;
\end{aligned}
\qquad \text{(A-8)}
$$

where P^* is a reference pressure, d is the depth of the model layer, and τ is a representative time scale to be defined later.

Substitution of (A-8) into (A-1) through (A-5) yields the non-dimensional set

$$\frac{du}{dt} = -\frac{\Theta\theta c_p^*\tau^2}{d^2}\frac{\partial\pi}{\partial x} + av + K_x\frac{\partial^2 u}{\partial x^2} + K_z\frac{\partial^2 u}{\partial z^2}, \qquad \text{(A-9)}$$

$$\frac{dv}{dt} = -au + K_x\frac{\partial^2 v}{\partial x^2} + K_z\frac{\partial^2 v}{\partial z^2}, \qquad \text{(A-10)}$$

$$\frac{dw}{dt} = -\frac{\Theta\theta c_p^*\tau^2}{d^2}\frac{\partial\pi}{\partial z} - g + K_x\frac{\partial^2 w}{\partial x^2} + K_z\frac{\partial^2 w}{\partial z^2}, \qquad \text{(A-11)}$$

$$\frac{d}{dt}[(1 - c_p^*/R^*) \ln \pi + \ln \theta] = \frac{\partial u}{\partial x} + \frac{\partial w}{\partial z}; \tag{A-12}$$

$$\frac{d\theta}{dt} = \frac{\Phi}{s} + K_x \frac{\partial^2 \theta}{\partial x^2} + K_z \frac{\partial^2 \theta}{\partial z^2}, \tag{A-13}$$

where now only the parameters Θ, c_p^*, R^*, τ, and d have dimensions.

In the lower atmosphere the variation of potential temperature from a constant value is generally small, usually no more than 30K. This is only about one-tenth the mean value of potential temperature in that region. We make use of that fact by defining

$$\theta = 1 + O(\epsilon) \tag{A-14}$$

where

$$\epsilon = \Delta\theta^*/\Theta \sim 1/10. \tag{A-15}$$

It will be convenient to have the radiation term also expressed in potential temperature. Let us determine how much error is introduced if we substitute θ^* for T^* in the first term of (A-5). From (A-8) we may estimate the value of π for this model which is applied to motions in a layer 1 km thick near the bottom of the atmosphere, say, between 900 and 800 mb. For such a layer, $\pi = 0.97 = 1 + O(\delta)$. Thus,

$$T^* = \Theta\theta(1 + O(\delta)), \tag{A-16}$$

or non-dimensional temperature is

$$T = T^*/\Theta = \theta(1 + O(\delta)). \tag{A-17}$$

Since $\delta \sim 1/100$, we see that non-dimensional temperature is equal to

θ to a closer degree of accuracy than is θ equal to one. This equivalence of temperature and potential temperature in shallow layers will be discussed later on in connection with the entire set of equations. Upon making the substitution of θ for T in (A-7) and inserting the result in (A-13), we have

$$\frac{d\theta}{dt} = -4\kappa\sigma\Theta^3\theta^4/s + K_x\frac{\partial^2\theta}{\partial x^2} + K_z\frac{\partial^2\theta}{\partial z^2} . \qquad (A-18)$$

Ogura and Phillips, along with other investigators, have shown that high-frequency acoustic waves are effectively eliminated from the solutions of the governing equations by the proper choice of time scale, τ. That choice is determined by the Brunt-Väisälä frequency which is the rate at which a disturbed parcel of air will oscillate vertically about its mean position in a stably-stratified environment. The expression of that frequency is

$$N^2 = \frac{g^*}{\theta^*}\frac{\partial\theta^*}{\partial z^*} \approx \frac{g^*}{\Theta}\frac{\Delta\theta^*}{d} \approx \frac{g^*\epsilon}{d} . \qquad (A-19)$$

Since the depth of our model is d = 1 km, the time scale necessary to eliminate acoustic waves is

$$\tau = N^{-1} \approx (d/g^*\epsilon)^{1/2} \approx 35 \text{ sec.} \qquad (A-20)$$

We define for convenience

$$\mu = g^*d/c_p^*\Theta = d/h \qquad (A-21)$$

where $h = c_p^* \Theta / g^*$ is the depth of an isentropic atmosphere of potential temperature Θ. For typical Θ in the troposphere, h is approximately 30 km.

With substitutions (A-20) and (A-21), we may now write (A-9) through (A-11) as

$$\epsilon\mu \frac{du}{dt} = -\theta \frac{\partial \pi}{\partial x} + \epsilon\mu a v + \epsilon\mu K_x \frac{\partial^2 u}{\partial x^2} + \epsilon\mu K_z \frac{\partial^2 u}{\partial z^2}, \qquad \text{(A-22)}$$

$$\epsilon\mu \frac{dv}{dt} = - \epsilon\mu a u + \epsilon\mu K_x \frac{\partial^2 v}{\partial x^2} + \epsilon\mu K_z \frac{\partial^2 v}{\partial z^2}, \qquad \text{(A-23)}$$

$$\epsilon\mu \frac{dw}{dt} = -\theta \frac{\partial \pi}{\partial z} - \mu + \epsilon\mu K_x \frac{\partial^2 w}{\partial x^2} + \epsilon\mu K_z \frac{\partial^2 w}{\partial z^2}. \qquad \text{(A-24)}$$

We now expand the dependent variables as power series in ϵ:

$$\begin{aligned} u &= u_0 + \epsilon u_1 + \epsilon^2 u_2 + \ldots \\ v &= v_0 + \epsilon v_1 + \epsilon^2 v_2 + \ldots \\ w &= w_0 + \epsilon w_1 + \epsilon^2 w_2 + \ldots \\ \pi &= \pi_0 + \epsilon \pi_1 + \epsilon^2 \pi_2 + \ldots \\ \theta &= \theta_0 + \epsilon \theta_1 + \epsilon^2 \theta_2 + \ldots . \end{aligned} \qquad \text{(A-25)}$$

By inserting (A-25) into (A-22) through (A-24), we get a set of zero-order equations which is identical to that derived by Ogura and Phillips. That is, the zero-order terms express the pressure distribution in a hydrostatic atmosphere of uniform potential temperature Θ:

$$\pi_0(z) = \pi_0(0) - \mu z, \qquad \text{(A-26)}$$

where $\pi_0(0)$ is a constant pressure taken, for convenience, to be equal to one at the lower boundary. Also,

$$\rho_0 = (P^*/R^*\Theta)\,\pi_0^{(c_p^*/R^*)-1} . \qquad \text{(A-27)}$$

With (A-26) and (A-27), the zero-order terms of the equation of continuity (A-12) may be written

$$\frac{\partial(\rho_0 u_0)}{\partial x} + \frac{\partial(\rho_0 w_0)}{\partial z} = 0. \qquad \text{(A-28)}$$

The first-order terms of ϵ in (A-22) through (A-24) yield

$$\mu \frac{du_0}{dt} = -\frac{\partial \pi_1}{\partial x} + \mu a v_0 + \mu K_x \frac{\partial^2 u_0}{\partial x^2} + \mu K_z \frac{\partial^2 u_0}{\partial z^2}, \qquad \text{(A-29)}$$

$$\mu \frac{dv_0}{dt} = -\mu a u_0 + \mu K_x \frac{\partial^2 v_0}{\partial x^2} + \mu K_z \frac{\partial^2 v_0}{\partial z^2}, \qquad \text{(A-30)}$$

$$\mu \frac{dw_0}{dt} = -\frac{\partial \pi_1}{\partial z} + \mu \theta_1 + \mu K_x \frac{\partial^2 w_0}{\partial x^2} + \mu K_z \frac{\partial^2 w_0}{\partial z^2}, \qquad \text{(A-31)}$$

where

$$\frac{d}{dt} = \frac{\partial}{\partial t} + u_0 \frac{\partial}{\partial x} + w_0 \frac{\partial}{\partial z} . \qquad \text{(A-32)}$$

In the thermodynamic equation (A-18), the zero-order terms of ϵ are identically equal to zero. Upon expanding the fourth power of θ in a series and collecting the first-order terms in μ, we have

$$\frac{d\theta_1}{dt} = -\frac{4\kappa\sigma\Theta^3}{\epsilon s} - \frac{16\kappa\sigma\Theta^3\theta_1}{s} + K_x \frac{\partial^2 \theta_1}{\partial x^2} + K_z \frac{\partial^2 \theta_1}{\partial z^2} . \qquad \text{(A-33)}$$

Inclusion of the first term on the right in (A-33) is cautionary. It may have the same magnitude as ϵ. Goody has estimated $\kappa = 2 \times 10^{-2}$ cm^{-1} for water vapor at S. T. P. while admitting an order of magnitude uncertainty. Since water vapor is the principal absorber of radiation within the lower atmosphere, we may apply that value of κ to estimate the maximum value of the first term. Upon inserting the known values of σ, s, and Θ, we find the first term equals 0.16 which is comparable to ϵ. Therefore, we shall carry that term until we can find better justification for neglecting it.

Equations (A-28) through (A-31) and (A-33) form what is known as an "anelastic" or soundproof set by virtue of the fact that the energy integral formed from them is devoid of elastic energy.

The nature of the problem being attacked allows further simplification of the governing equations. Because the convection is confined to a shallow layer in the atmosphere (d = 1 km), we may make use of the fact that $\mu = d/h << 1$. We expand the dependent variables in a series in μ:

$$u_0 = u_{00} + \mu u_{01} + \ldots \tag{A-34}$$

with similar expressions for v_0, w_0, θ_1, π_0, π_1, and ρ_0. Upon the substitution of those expansions into (A-26) and then (A-27), we obtain

$$\pi_{00} = 1, \qquad \pi_{01} = -z,$$

and

$$\rho_{00} = (P^*/R^*\Theta) = \text{constant}. \tag{A-35}$$

The zero-order terms of (A-29) through (A-31) give π_{10} equal to a constant which we shall take as zero for convenience. The first-order terms of (A-29) through (A-31) form the set

$$\frac{du_{00}}{dt} = -\frac{\partial \pi_{11}}{\partial x} + \alpha v_{00} + K_x \frac{\partial^2 u_{00}}{\partial x^2} + K_z \frac{\partial^2 u_{00}}{\partial z^2}, \tag{A-36}$$

$$\frac{dv_{00}}{dt} = -\alpha u_{00} + K_x \frac{\partial^2 v_{00}}{\partial x^2} + K_z \frac{\partial^2 v_{00}}{\partial z^2}, \tag{A-37}$$

$$\frac{dw_{00}}{dt} = -\frac{\partial \pi_{11}}{\partial z} + \theta_{10} + K_x \frac{\partial^2 w_{00}}{\partial x^2} + K_z \frac{\partial^2 w_{00}}{\partial z^2}. \tag{A-38}$$

Because of (A-35), the continuity equation (A-28) reduces to

$$\frac{\partial u_{00}}{\partial x} + \frac{\partial w_{00}}{\partial z} = 0, \tag{A-39}$$

and (A-33) becomes

$$\frac{d\theta_{10}}{dt} = -B - A\theta_{10} + K_x \frac{\partial^2 \theta_{10}}{\partial x^2} + K_z \frac{\partial^2 \theta_{10}}{\partial z^2}, \tag{A-40}$$

where

$$B = 4\kappa\sigma\Theta^3/\epsilon s$$

and

$$A = 16\kappa\sigma\Theta^3/s = 4\epsilon B. \tag{A-41}$$

The operator d/dt is now defined

$$\frac{d}{dt} = \frac{\partial}{\partial t} + u_{00}\frac{\partial}{\partial x} + w_{00}\frac{\partial}{\partial z}. \tag{A-42}$$

Ogura and Phillips point out that in the resultant set of governing equations, π_{11} is the deviation of pressure from that of an adiabatic atmosphere, and θ_{10} is the deviation of temperature from that of an adiabatic atmosphere. This is easily verified by expanding the definitions of π and T^* given in (A-8) along with (A-14) and the equation of state, $p = \rho RT$, in terms of ϵ and μ.

The set of equations (A-36) through (A-38) are similar in form to those of the incompressible Boussinesq system used in many studies of small-scale convection in which density variations are neglected except as they modify the influence of gravity in producing bouyancy. Also, because we have not considered the release of latent heat in the thermodynamic equation, solutions for π_{11} may be obtained. When moisture is included in a convective model, an implicit relationship exists between θ_1, and π_1, and the rate of release of latent heat. For shallow, moist convection, the equations may be solved because θ_{10} (actual temperature) is independent of π_{11} (the dynamic pressure). However, inclusion of moisture in the present model, while eventually desirable would only serve to complicate the effects of large-scale subsidence on the convection.

We now linearize the set of governing equations by the usual perturbation technique. That is, we assume the total variation of the dependent variables can be represented by a mean or basic value plus some small deviation from that mean. By this we may neglect products of perturbation quantities on the basis of their magnitudes. To lessen complication of the notation, we shall drop all the subscripts in writing (A-36) through (A-40) in perturbation form, so that

$$
\begin{aligned}
u &= \overline{u} + u', \\
v &= \overline{v} + v', \\
w &= \overline{w} + w', \\
\pi &= \overline{\pi} + \pi', \\
\theta &= \overline{\theta} + \theta'.
\end{aligned}
\tag{A-43}
$$

Furthermore, to fit the model being studied, we shall specify

$$
\begin{aligned}
\overline{u} &= 0, \\
\overline{v} &= 0, \\
\overline{w} &= \text{constant}, \\
\overline{\pi} &= \overline{\pi}(z), \\
\overline{\theta} &= \overline{\theta}(z).
\end{aligned}
\tag{A-44}
$$

Using the expansions in (A-42) and (A-43) under the conditions (A-44), the governing set (A-36) through (A-40) reduce to equations (1) through (5) in Chapter II.

APPENDIX B

DERIVATION OF BASIC-STATE TEMPERATURE

The condition imposed upon the temperature distribution in the basic state is that it remain constant in time. Physically, in a layer throughout which adiabatic warming is taking place due to uniform subsidence of air, sufficient cooling must occur via turbulent exchanges of heat and by radiation. Under these conditions we may obtain an equation specifying the basic temperature distribution from (A-40), (A-42), and (A-43):

$$K_z \frac{d^2\overline{\theta}}{dz^2} - \overline{w}\frac{d\overline{\theta}}{dz} - A\overline{\theta} = B. \qquad \text{(B-1)}$$

Since (B-1) is an ordinary second-order differential equation with constant coefficients, it has a general solution

$$\overline{\theta} = -\frac{B}{A} + C_1 \exp\left[\frac{-\overline{w} + (\overline{w}^2 + 4AK_z)^{1/2}}{2K_z} \cdot z\right]$$

$$+ C_2 \exp\left[\frac{-\overline{w} - (\overline{w}^2 + 4AK_z)^{1/2}}{2K_z} \cdot z\right]. \qquad \text{(B-2)}$$

Under dry atmospheric conditions, the usual radiative cooling rate in the lower atmosphere is of the order 1 to 5C day^{-1} (Möller, 1951). Recalling that $\overline{\theta}$ is a deviation temperature, we estimate its magnitude in the layer to be 3C. For a cooling rate of 2.5C day^{-1}, $B \approx 10^{-5}$C sec^{-1}. Then by (A-41), $A \approx 4 \times 10^{-6}$ sec^{-1}.

An estimate of the heating effect due to subsidence in the layer is obtained by noting that the usual magnitudes of $\overline{w}$ are of order 1 to 5 cm sec^{-1} while typical temperature inversions have gradients of 1 to 10C km^{-1}. This is an order of magnitude larger than the radiation effect and indicates that the major cooling comes from the eddy conduction term. Therefore, instead of using the complete solution (B-2) to determine $\overline{\theta}$, we may justifiably neglect the radiation effect and choose a simpler form: that is,

$$\overline{\theta} = \overline{\theta}_o \left[\frac{e^{bz} - e^{b}}{1 - e^{b}} \right], \quad 0 \leqq z \leqq 1, \tag{B-3}$$

with $b = \overline{w}/K_z$ and $\overline{w} < 0$. Eq. (B-3) is the solution of (B-1) with $A = B = 0$ and under the boundary conditions that $\overline{\theta} = \overline{\theta}_o$ at $z = 0$; $\overline{\theta} = 0$ at $z = 1$. Numerically, with $\overline{w} = -1.5$ cm sec^{-1} and $K_z = 5 \times 10^4$ cm^2 sec^{-1}, the distributions of $\overline{\theta}$ calculated from (B-2) and (B-3) are nearly identical save for the constant B/A. Since $\overline{\theta}_o$ is an arbitrary choice, no generality is lost by neglecting B and A here.

APPENDIX C

INVESTIGATION OF COMPUTATIONAL STABILITY

Since excess temperature is the driving force for the convective model, we shall use (20) to investigate the requirements for computational stability. The other governing equations are of similar form, so the results of the investigation should be applicable to the entire set.

We assume that

$$T(m, n+1) = G\,T(m, n) \tag{C-1}$$

where G is an unknown amplification factor which must be less than or equal to one for computational stability. We further assume solutions to (20) of the form

$$T(m, n) \doteq E(t)\, e^{ijm\Delta z} \tag{C-2}$$

and

$$W(m, n) = F(t)\, e^{ijm\Delta z} \tag{C-3}$$

for m = 0, 1, 2, . . . , M. In (C-2) and (C-3), $i = (-1)^{1/2}$ and j is a vertical integer wave number.

By use of the above relationships, we may write (20) as

$$G = a + b(e^{ij\Delta z} + e^{-ij\Delta z}) - c(e^{ij\Delta z} - e^{-ij\Delta z}), \tag{C-4}$$

where

$$a = 1 - (k^2K_x\Delta t + 2b + A\Delta t + \beta\Delta tF/E)$$

$$= 1 - \xi , \quad \xi << 1, \tag{C-5}$$

$$b = K_z\Delta t/(\Delta z)^2, \tag{C-6}$$

$$c = \overline{w}\Delta t/2\Delta z . \tag{C-7}$$

Reverting to the trigonometric forms,

$$G = a + 2b \cos j\Delta z - i2c \sin j\Delta z . \tag{C-8}$$

We see that G is an imaginary number whose magnitude must be less than or equal to one. Thus, we require

$$G^2 = (a + 2b \cos j\Delta z)^2 + 4c^2 \sin^2 j\Delta z \leqq 1. \tag{C-9}$$

Consider those solution for which $\cos j\Delta z = \pm 1$. Then, $\sin j\Delta z = 0$, and

$$(a \pm 2b)^2 - 1 \leqq 0. \tag{C-10}$$

By substituting for a from (C-5), expanding, and rewriting, (C-10) becomes

$$(\xi \mp 2b)^2 \leqq 2(\xi - 2b). \tag{C-11}$$

Extracting the time increment, Δt, from both sides yields

$$\Delta t \leqq \frac{2}{\left(\frac{\xi \mp 2b}{\Delta t}\right)} . \tag{C-12}$$

Since both ξ and b are positive, (C-12) has a smallest value when the positive sign is taken in the parentheses. Hence, an estimate of the requirement for the computational stability of (20) is obtained from

$$\Delta t \leqq 2/(k^2K_x + 4K_z/(\Delta z)^2 + A + \beta F/E) \tag{C-13}$$

by using the values of the bracketed parameters assigned in Table 2 with β_{max} determined from (6):

$$\beta_{max} \approx 30 \times 10^{-5} \mathrm{C\ cm}^{-1}. \tag{C-14}$$

For 100-km wave length, $k^2 = 40 \times 10^{-14}\ \mathrm{cm}^{-2}$ and $F/E \sim w'/\theta' \sim 10$. Thus, the requirement for Δt is estimated as

$$\Delta t \leqq 57 \text{ sec.} \tag{C-15}$$

Since the stability requirement is wave-length dependent, we should be guided by the smallest expected value of the right side of (C-13) in the model application. Evaluating (C-14) for the 1-km wave length with $k^2 = 40 \times 10^{-10}\ \mathrm{cm}^{-2}$ and $F/E \sim w'/\theta' \sim 100$ gives a

$$\Delta t \leqq 24 \text{ sec.} \tag{C-16}$$

As an additional check, we may look at those solutions of (C-9) for which $\sin j\Delta z = \pm 1$ and $\cos j\Delta z = 0$. Then

$$a^2 + 4c^2 \leqq 1, \tag{C-17}$$

or, using (C-5),

$$(1 - \xi)^2 \leqq 1 - 4c^2 . \tag{C-18}$$

By making use of the binomial expansion of the left side of (C-18), we may write

$$1 - 2\xi \leqq 1 - 4c^2 , \tag{C-19}$$

or

$$c^2 \leqq \xi/2. \tag{C-20}$$

Thus,

$$\Delta t \leqq \frac{2(\Delta z)^2}{\bar{\bar{w}}^2} \left[k^2 K_x + \frac{2K_z}{(\Delta z)^2} + A + \frac{\beta F}{E} \right]. \tag{C-21}$$

For the largest scale (100 km), the right side of (C-21) has its smallest magnitude, and the stability requirement is

$$\Delta t \leqq 1.1 \times 10^5 \text{ sec}; \qquad \text{(C-22)}$$

a condition easily satisfied.

While (C-13) is only an estimate of the stability requirements for the numerical solutions, it is only slightly more restrictive than the requirement for a classical diffusion equation (see Dingle and Young, 1965); that is,

$$\Delta t \leqq (\Delta z)^2 / 2K_z . \qquad \text{(C-23)}$$

A conservative assignment of Δt less than half that required by (C-13) should insure stable solutions with small truncation errors.

APPENDIX D

RECURSION FORMULA FOR $\psi(z, t)$

The solution of (10) usually requires two-dimensional relaxation techniques under suitable boundary conditions. However, because of the horizontal periodicity of our model, (10) reduces to (15) which is solved by a simple set of algebraic recursion formulas.

For simplicity, we shall consider here a one-dimensional form of (15) denoted by

$$H(z) = k^2\psi(z) - \frac{d^2\psi(z)}{dz^2} \quad . \tag{D-1}$$

A centered-difference scheme is used for the finite-difference form of (D-1):

$$H(m) = k^2\psi(m) - [\psi(m+1) + \psi(m-1) - 2\psi(m)]/(\Delta z)^2 \tag{D-2}$$

where $m = 2, 3, \ldots, M-1$; the total number of grid points being M. Rearranging (D-2),

$$a\psi(m) = \psi(m+1) + \psi(m-1) + bH(m) \tag{D-3}$$

with $a = 2 + bk^2$ and $b = (\Delta z)^2$.

Consider now that m is fixed at its smallest value such that $\psi(m-1)$ in (D-3) is the known lower boundary value. The H(m) have been previously determined by the step-wise integration of (18), (19), and (20). The only unknowns in (D-3) are $\psi(m)$ and $\psi(m+1)$.

We now write (D-3) for the $m+1^{th}$ grid point:

$$a\psi(m+1) = \psi(m+2) + \psi(m) + bH(m+1). \tag{D-4}$$

Upon eliminating $\psi(m)$ between (D-3) and (D-4), we get

$$(a^2 - 1)\,\psi(m+1) = a\psi(m+2) + abH(m+1) + bH(m) + \psi(m-1). \tag{D-5}$$

Let us now for convenience designate the coefficient of $\psi(m+1)$ as $S(m+1) = (a^2 - 1)$. Further, we will designate $R(m) = bH(m) + \psi(m+1)$. Then (D-5) may be written

$$S(m+1)\,\psi(m+1) = S(m)\,\psi(m+2) + S(m)bH(m+1) + R(m). \tag{D-6}$$

Since the last two terms of (D-6) contain only known parameters, we shall symbolize them by $R(m+1)$. We now write (D-3) for the $m+2^{th}$ grid point,

$$a\psi(m+2) = \psi(m+3) + \psi(m+1) + bH(m+2), \tag{D-7}$$

and eliminate $\psi(m+1)$ between (D-6) and (D-7) with the result

$$\begin{aligned}(aS(m+1) - S(m))\,\psi(m+2) &= S(m+1)\,\psi(m+3) \\ &\quad + S(m+1)bH(m+2) + R(m+1),\end{aligned} \tag{D-8}$$

or

$$S(m+2)\,\psi(m+2) = S(m+1)\,\psi(m+3) + R(m+2). \tag{D-9}$$

By continuing the process, one can see that the coefficients of the left-hand side of (D-9) for any given m will always be of the form

$$S(m) = aS(m-1) - S(m-2), \tag{D-10}$$

and the terms on the right which depend on $H(m)$ for their value can be written in the general form

$$R(m) = S(m-1)bH(m) + R(m-1). \qquad \text{(D-11)}$$

Equations (D-10) and (D-11) are general provided we make allowances for the case when m = 2. From (D-3), it is evident that the set of equations will be satisfied provided we take $S(1) = 1$, $S(0) = 0$, and $R(1) = \psi(1)$, the lower boundary value. Under those conditions, (D-9) may be put in the general form

$$\psi(m) = (S(m-1)\,\psi(m+1) + R(m))\,/\,S(m), \qquad \text{(D-12)}$$

$$m = 2,\ 3,\ 4,\ \ldots,\ M-1.$$

The solution of (D-12) is conveniently begun at $m = M-1$ with $\psi(m+1) = \psi(M)$, the upper boundary value which is taken as zero in this model. Prior to that calculation, however, it is necessary to determine the values of S and R by starting with m = 2 and proceeding upward.

Table 1

Nomenclature

Note: An asterisk means the parameter has its usual dimensions. All other parameters are non-dimensional unless stated contrariwise. Also, an overbar designates the basic-state parameters and a prime the perturbation parameters.

A	Coefficient of radiative cooling due to temperature deviation from that of an atmosphere of constant potential temperature.
ADKE	The change in volume-averaged kinetic energy by advection through the lower boundary.
ADPE	The change in volume-averaged available potential energy by advection through the lower boundary.
B	Radiative temperature change for atmosphere with constant potential temperature.
C	Degrees Celsius.
c_p^*, c_v^*	Specific heat capacities of air at constant pressure and volume, respectively.
d	Dimensional depth of the convective layer modeled.
f*	Coriolis parameter equal to twice the angular velocity of the earth times the sine of the latitude.
g*, g	Acceleration due to gravity.
H	Amplitude of horizontal vorticity perturbation.
h	Height of an atmosphere with constant potential temperature.
HDIF	Volume-averaged horizontal diffusion of total energy.
K	Degrees Kelvin; general horizontal eddy coefficient for turbulent exchanges.

Table 1 (continued)

K_x^*, K_x	Horizontal eddy coefficient for turbulent heat and momentum exchange.
K_z^*, K_z	Vertical eddy coefficient for turbulent heat and momentum exchange.
k	Horizontal wave number.
L	Horizontal wave length.
M	Number of grid points in the vertical direction.
N	Brunt-Väisälä frequency.
P^*, p^*	Reference pressure and actual pressure of atmosphere, respectively.
PRES	Work done by the perturbation motion against pressure forces along the lower boundary.
R	Summation parameter in recursion formula for solution of $\psi(z,t)$; non-dimensional gas constant for dry air.
R^*	Gas constant for dry air.
RAD	Volume-averaged radiative depletion of energy.
S	Summation parameter in recursion formula for solution of $\psi(z,t)$.
s^*, s	Heat content of air per unit volume per degree $(=\rho^* c_v^*)$.
T	Amplitude of horizontal temperature perturbation.
T^*	Absolute air temperature.
t^*, t	Time.
Δt	Time increment for numerical solutions.
u^*, u $\overline{u}$, u', U	Eastward (x) component of wind velocity. U is amplitude of horizontal perturbation.

Table 1 (continued)

v^*, v $\bar{v}$, v', V	Northward (y) component of wind velocity. V is amplitude of horizontal perturbation.
VDIF	Volume-averaged vertical diffusion of total energy.
w^*, w $\bar{w}$, w', W	Vertical (z) component of wind velocity. W is amplitude of horizontal perturbation.
x^*, x y^*, y z^*, z	Coordinate axes along eastward, northward, and vertical directions, respectively.
Δz	Vertical mesh size for numerical solutions.
α	Non-dimensional Coriolis parameter.
β	Static stability of basic state ($= \partial\bar{\theta}/\partial z$).
ϵ	The order of allowable deviations of the dependent variables from their values in an atmosphere with constant potential temperature ($=\Delta\theta/\Theta$).
η'	Vorticity perturbation about the negative y-axis.
Θ	Constant dimensional potential temperature representative of the model layer.
θ^*, θ	Potential temperature.
$\bar{\theta}$, θ'	Temperature deviation from that in an atmosphere of constant potential temperature.
κ^*, κ	Coefficient of absorption per unit volume.
μ	Ratio of depth of model layer, d, to height, h, of atmosphere with constant potential temperature.
π, $\bar{\pi}$ π', Π	Pressure deviation from that in an atmosphere with constant potential temperature. Π is amplitude of horizontal perturbation.
ρ^*, ρ	Air density.

Table 1 (continued)

σ^*, σ	Stefan's constant.
τ	Dimensional scale time necessary for the elimination of acoustic frequencies from solutions of the governing differential equations.
Φ^*, Φ	Radiative cooling rate of air per unit volume.
ψ', ψ	Streamfunction in the x-z plane and amplitude of horizontal perturbation, respectively.

Table 2

Constant Parameters

$A = 4 \times 10^{-6}\ \mathrm{sec}^{-1}$

$d = 1$ km

$K_x = 5 \times 10^{6}\ \mathrm{cm}^2\ \mathrm{sec}^{-1}$

$K_z = 5 \times 10^{4}\ \mathrm{cm}^2\ \mathrm{sec}^{-1}$

$T_o = 3$C

$\Delta z = 25$ m

$a = 10^{-4}\ \mathrm{sec}^{-1}$

$\Theta = 300$K

$\overline{\theta}_o = -10$C

$\tau = 34.7$ sec

Table 3

Parameters Varied for Individual Cases

L (km)	1	5	10	20	50	100
$\overline{w}$ (cm sec^{-1})	-1.5	-1.5	-1.5	-1.5	-1.5	-1.5
		-1.5×10^{-3}	-1.5×10^{-3}	-1.5×10^{-3}	-1.5×10^{-3}	-1.5×10^{-3}
Δt (sec)	2	6	6	6	12	12
Total run time (hr)	4	6	6	6	12	12
				12		

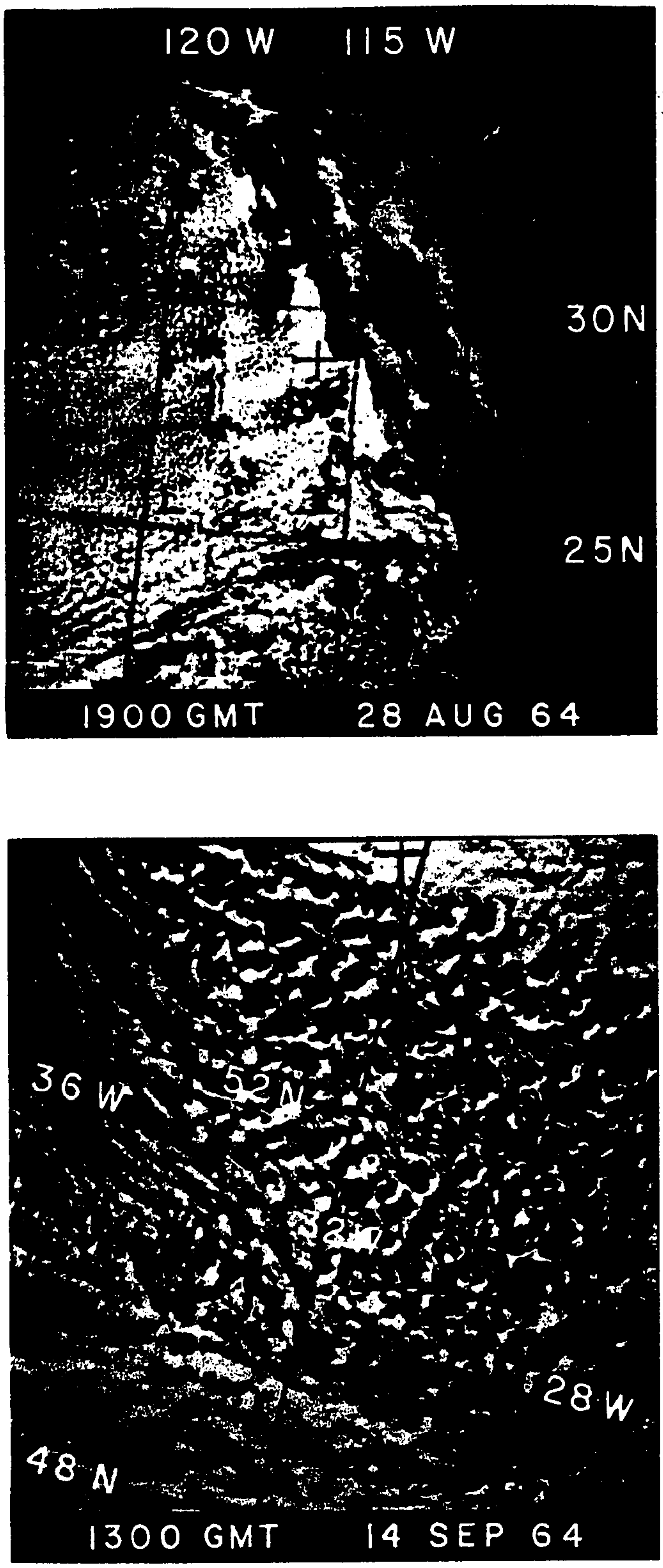

Fig. 1. Examples of cellular convective cloud patterns photographed from NIMBUS I satellite.

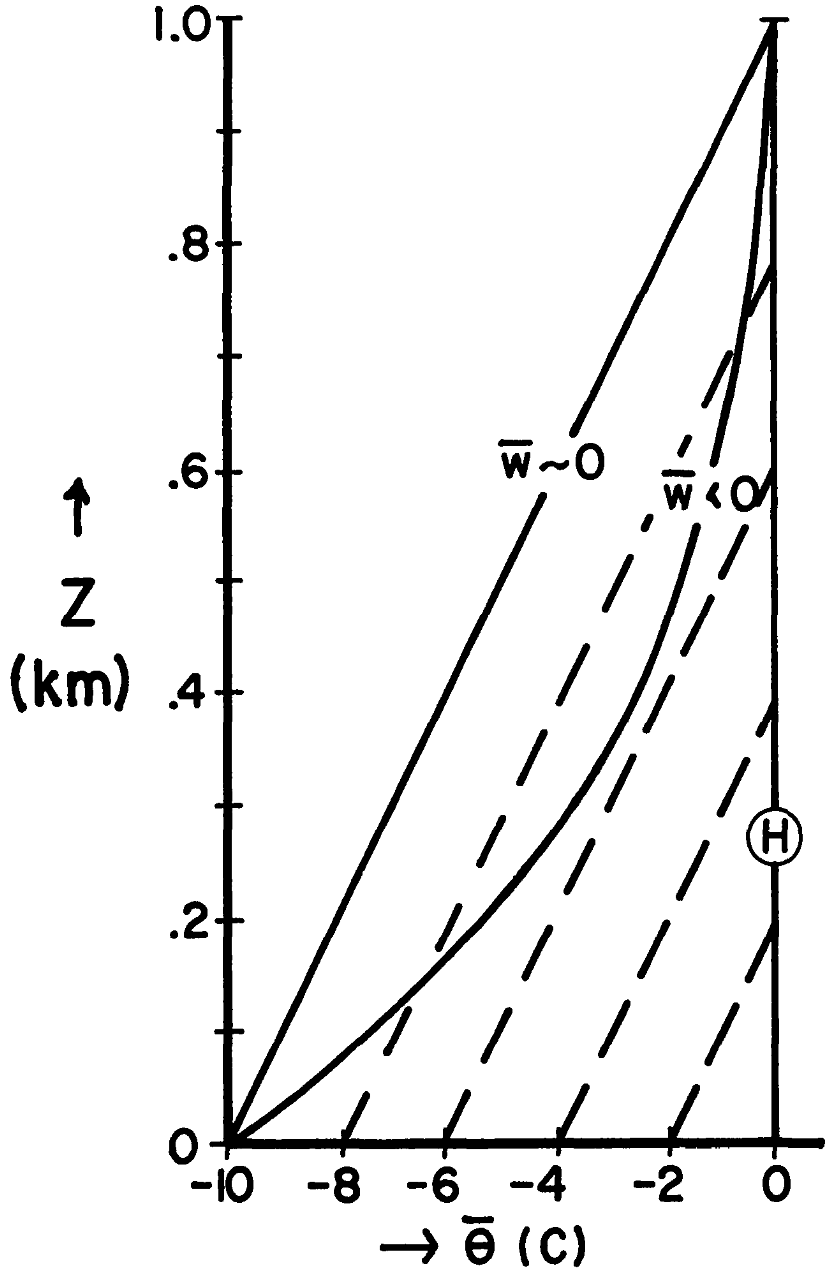

Fig. 2. Basic-state temperature distributions for subsidence and non-subsidence cases. Abscissa is deviation of basic state from the temperature in a layer with constant potential temperature Ⓗ. Dashed lines show orientation of absolute isotherms.

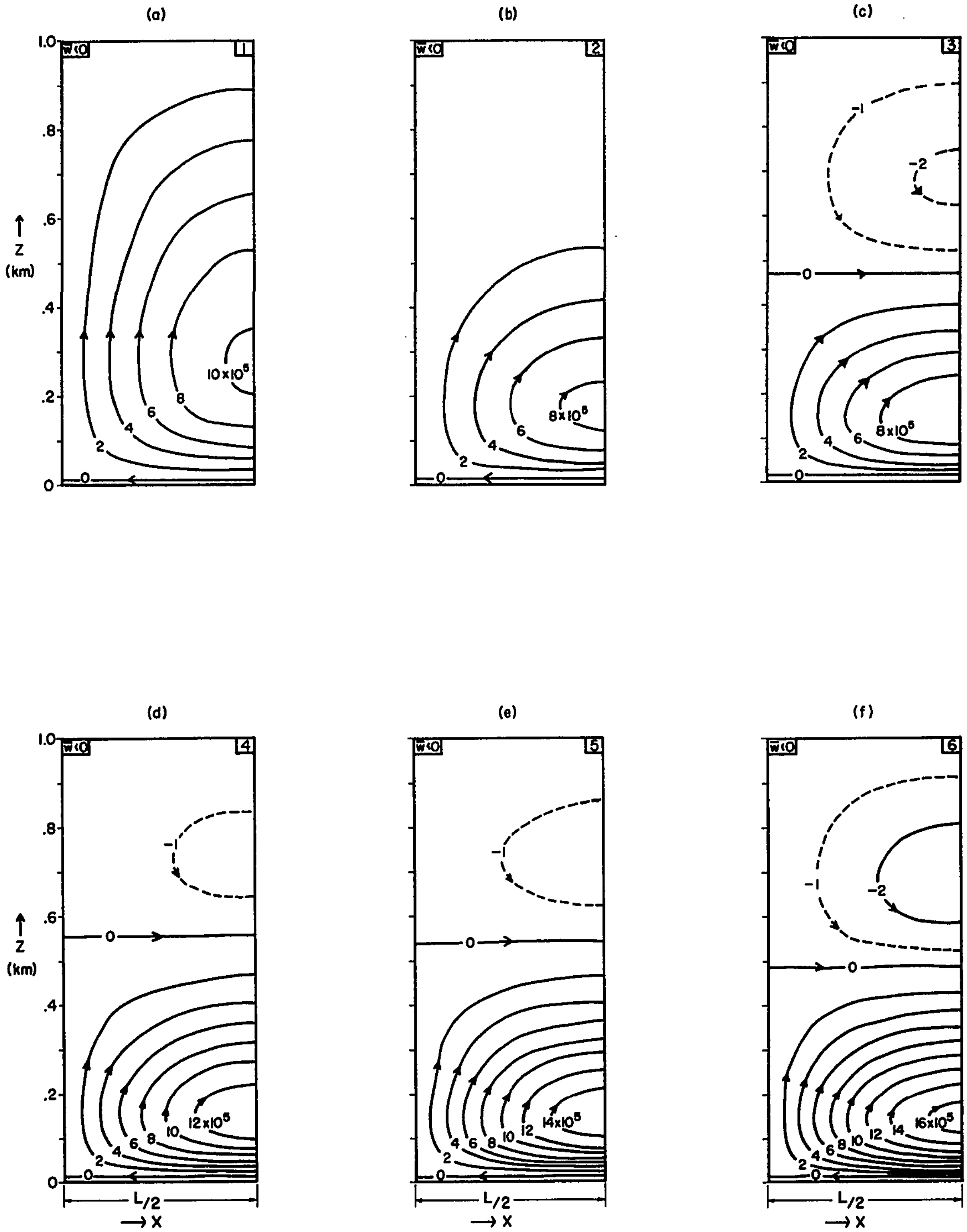

Fig. 3. Growth of streamfunction field during first six hours for wave length L = 20 km with subsidence. Units are 10^5 cm^2 sec^{-1}. Number in upper right of each diagram indicates time in hours.

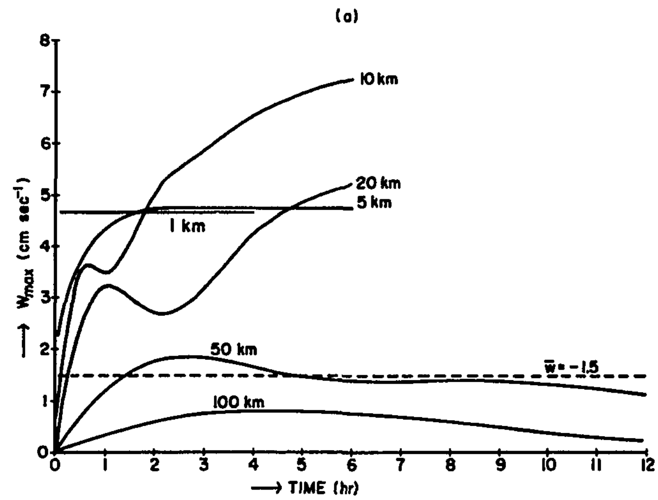

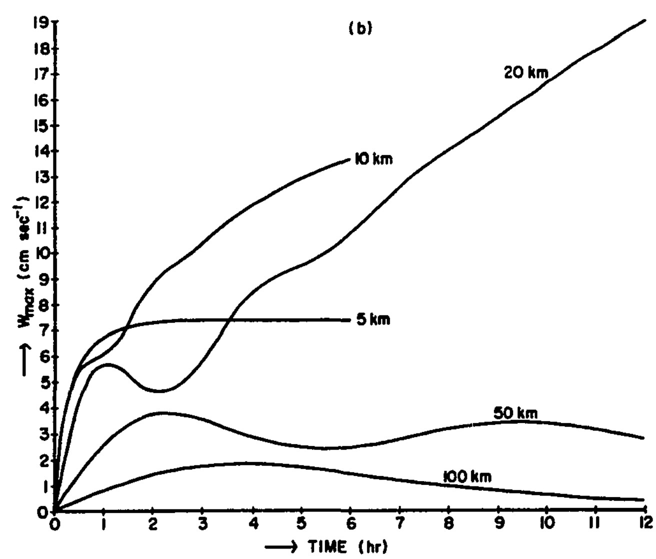

Fig. 4. Variation of W_{max} with time for different cases a) with subsidence and b) without subsidence.

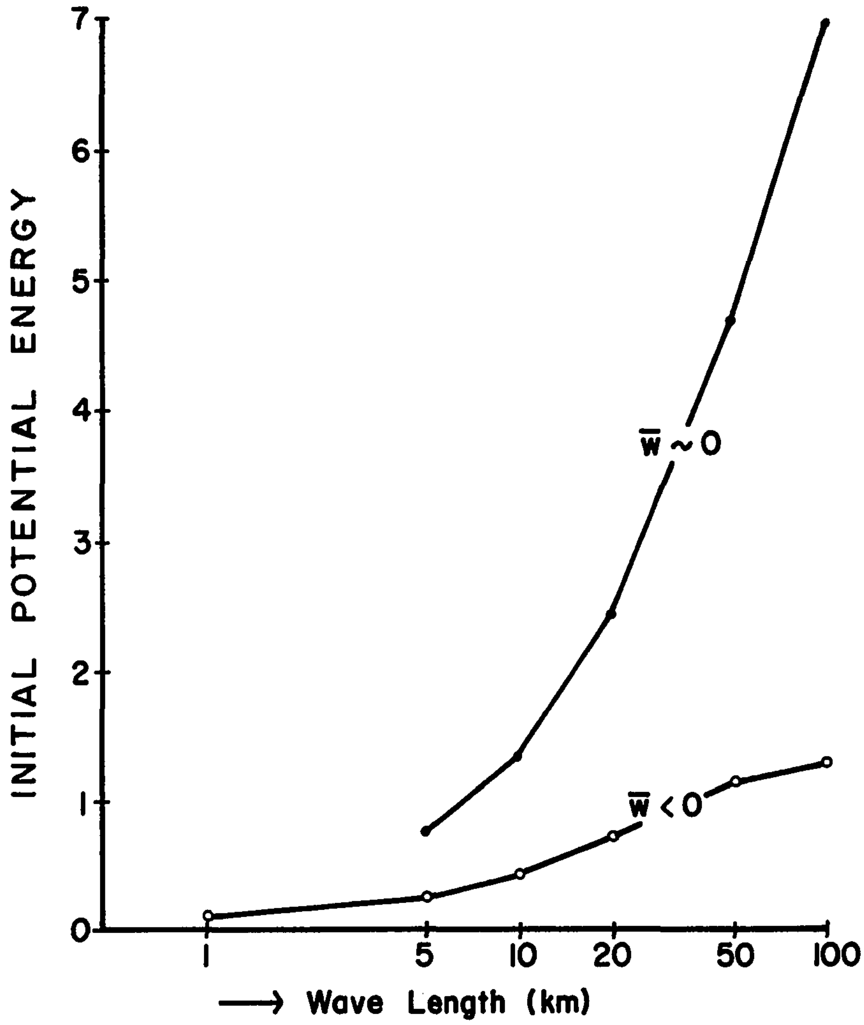

Fig. 5. Initial available potential energy in arbitrary units for cases with and without subsidence.

(a)

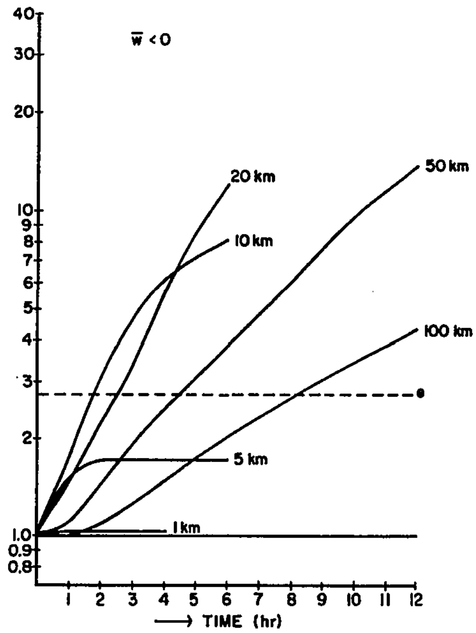

(b)

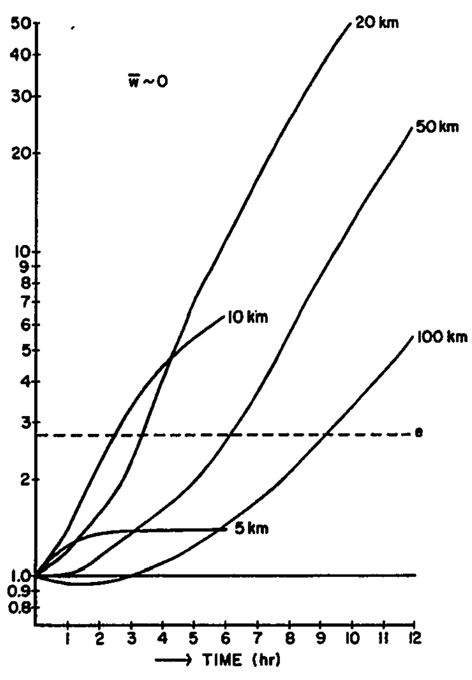

Fig. 6. Ratio of total energy to initial energy as a function of time for a) subsidence cases and b) non-subsidence cases.

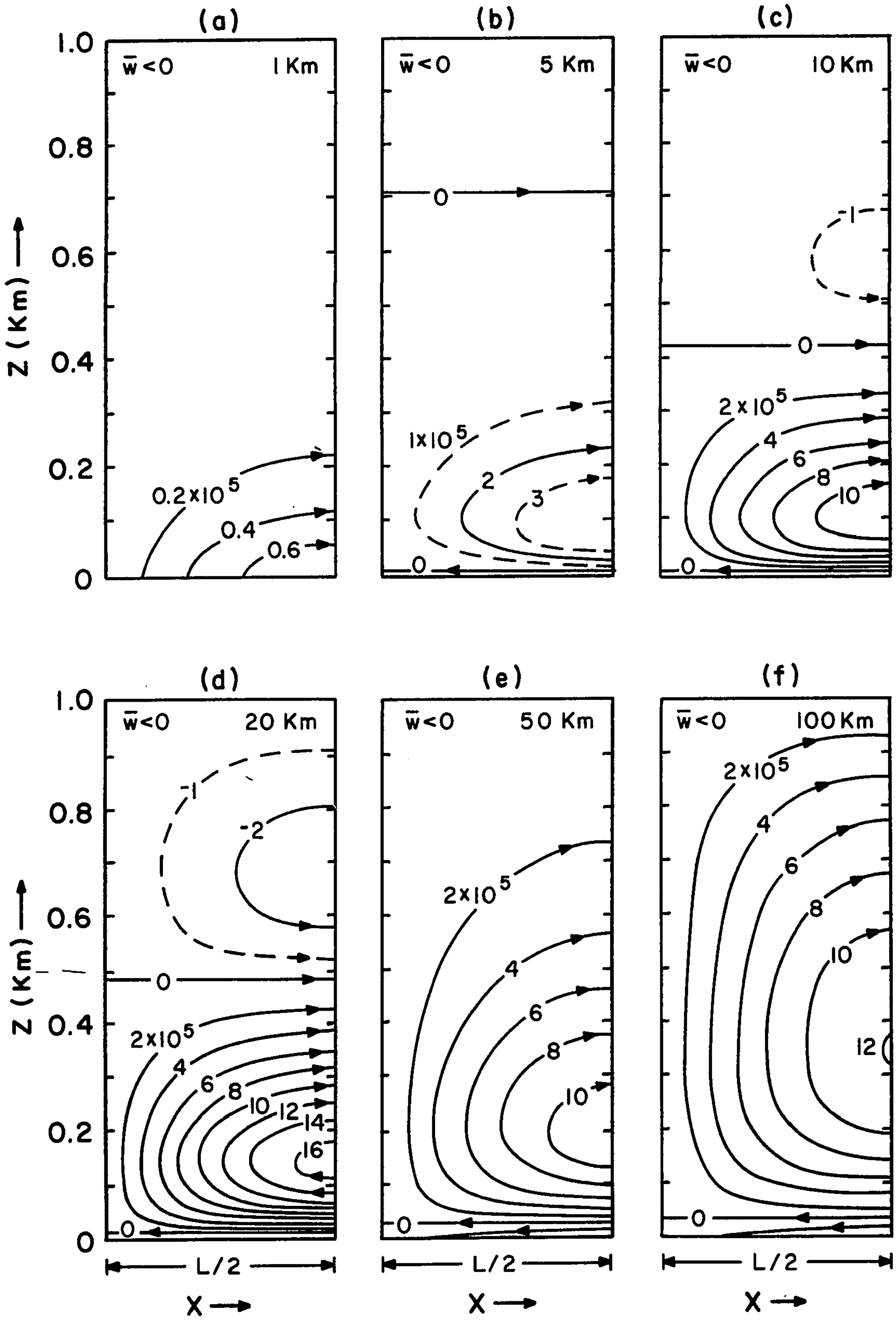

Fig. 7. Streamfunction at t = 6 hr for subsidence cases. Units are 10^5 cm^2 sec^{-1}.

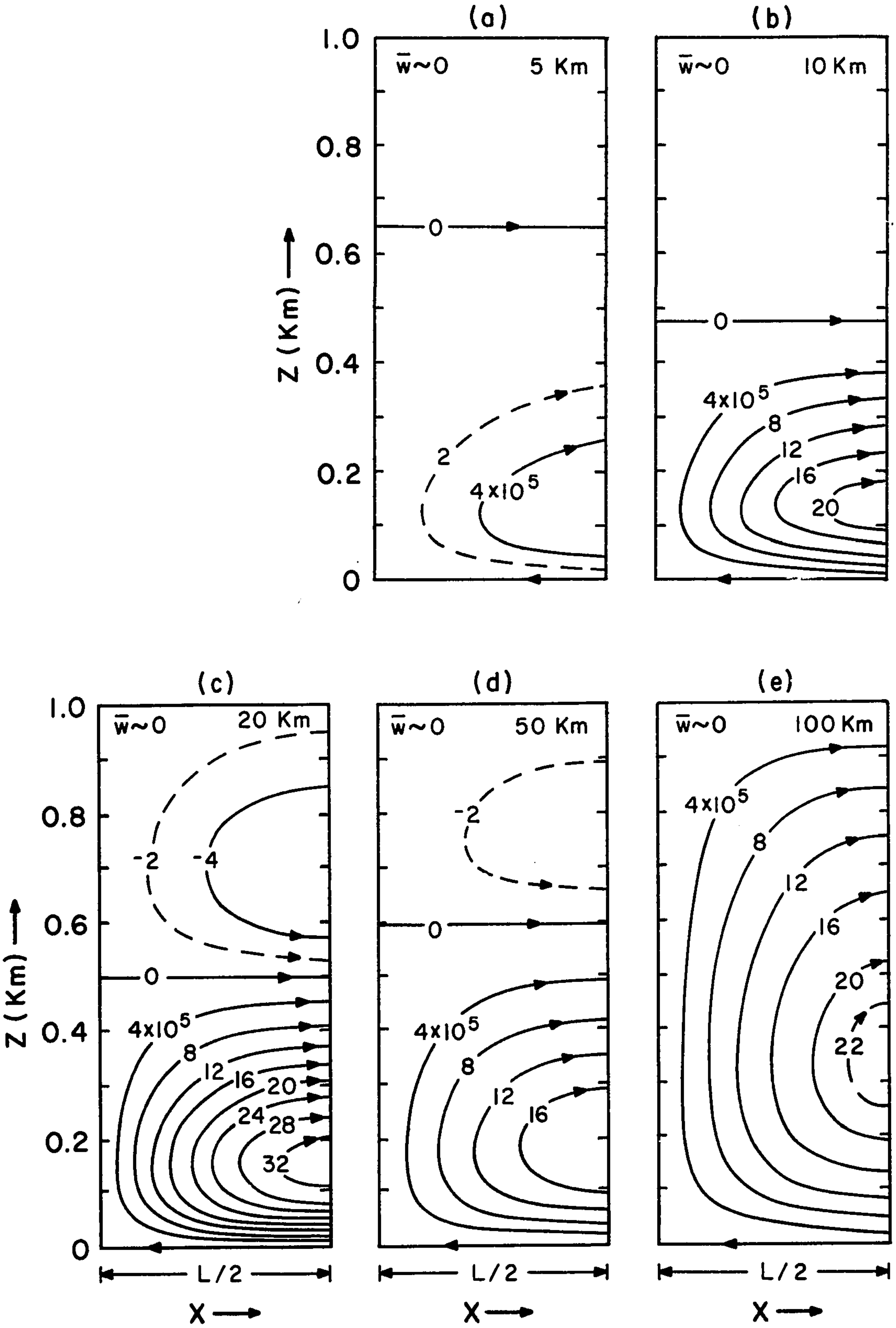

Fig. 8. Streamfunction at t = 6 hr for non-subsidence cases. Units are 10^5 cm^2 sec^{-1}.

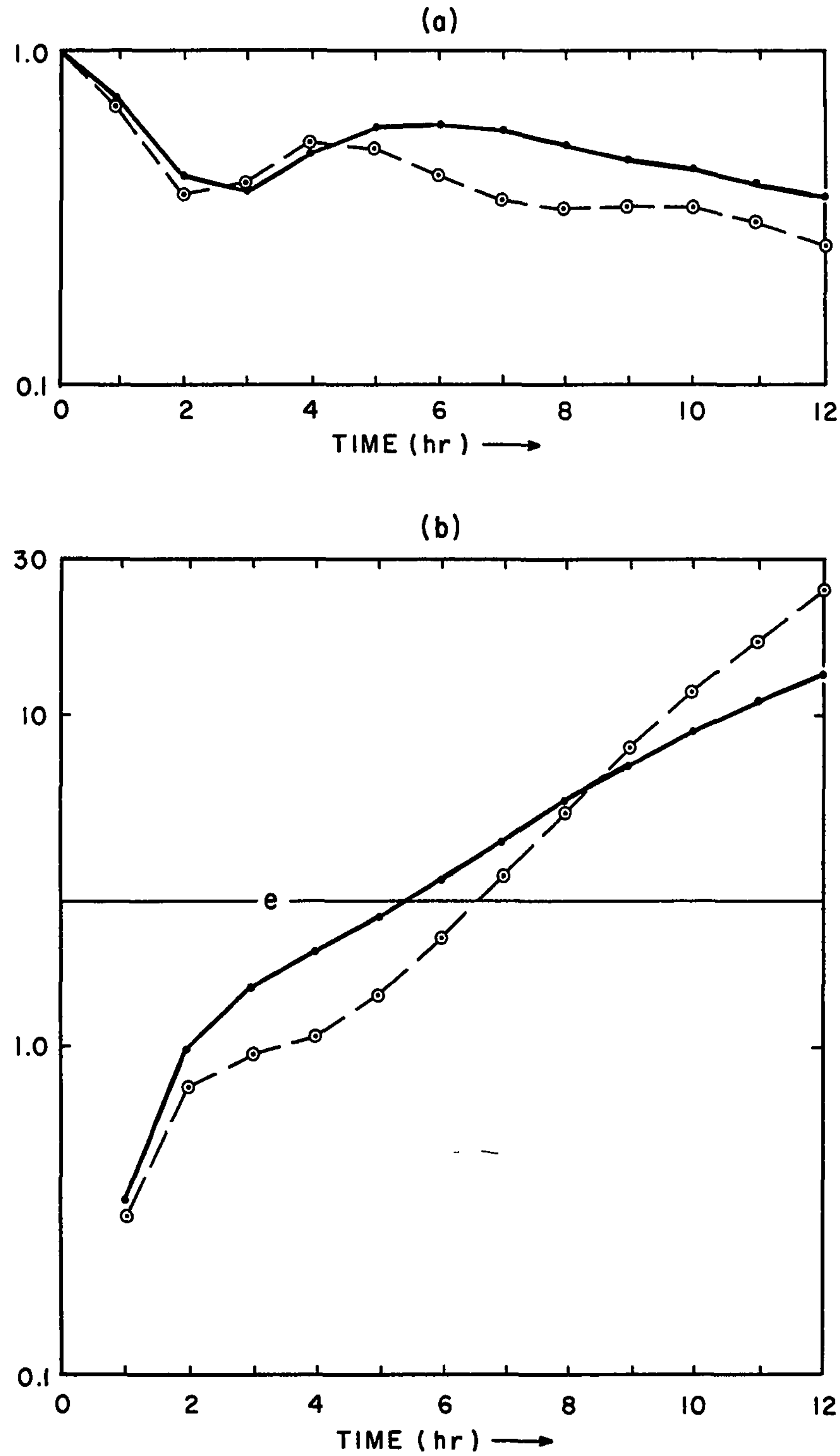

Fig. 9. Time variation of a) available potential energy and b) kinetic energy expressed as a fraction of the initial energy for the 50-km cases. Solid lines are for subsidence case; dashed lines for non-subsidence case.

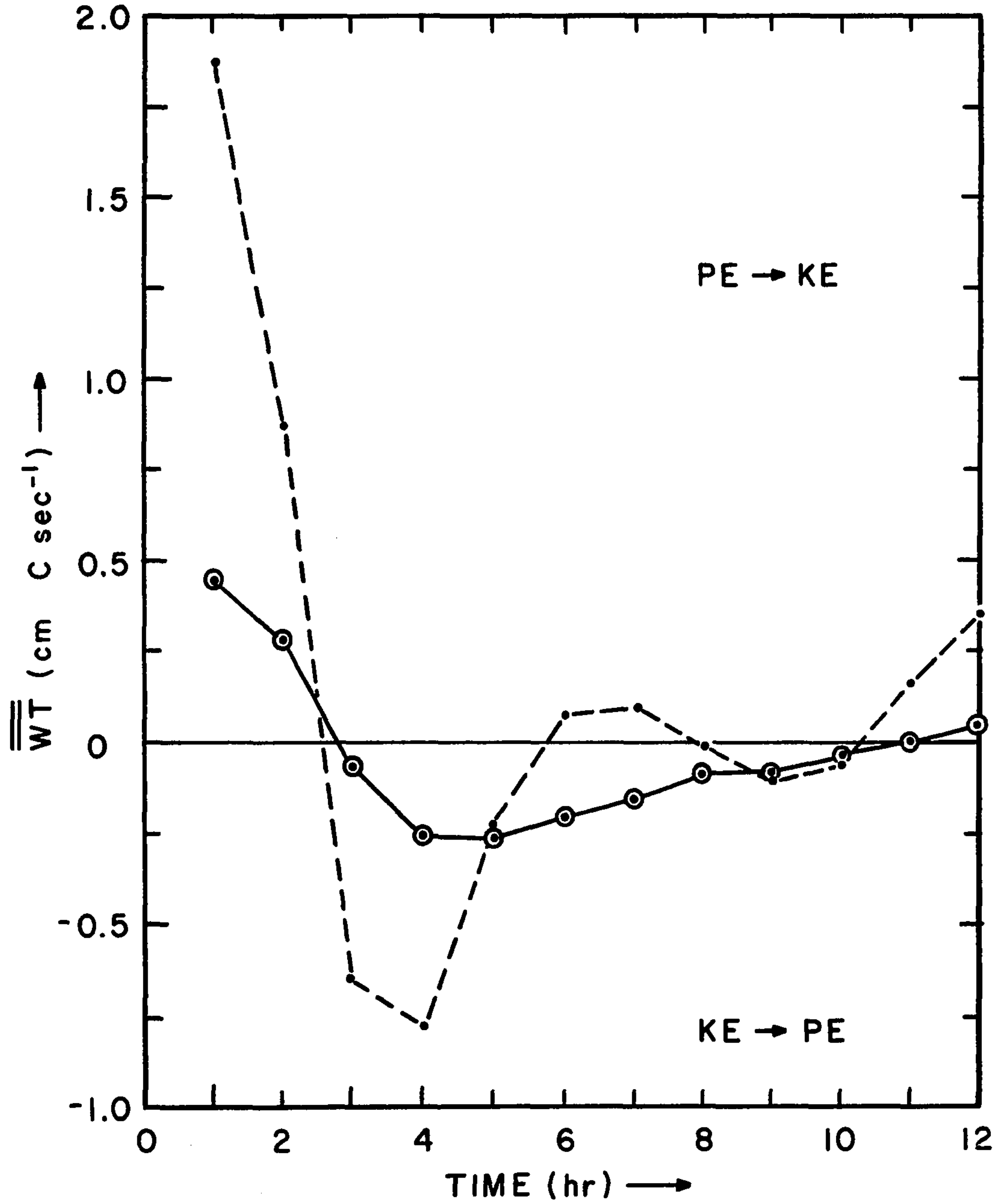

Fig. 10. Vertically-averaged convective heat transport for the 50-km cases. Solid line for subsidence case; dashed line for non-subsidence case. Positive values indicate potential energy is converting to kinetic energy.

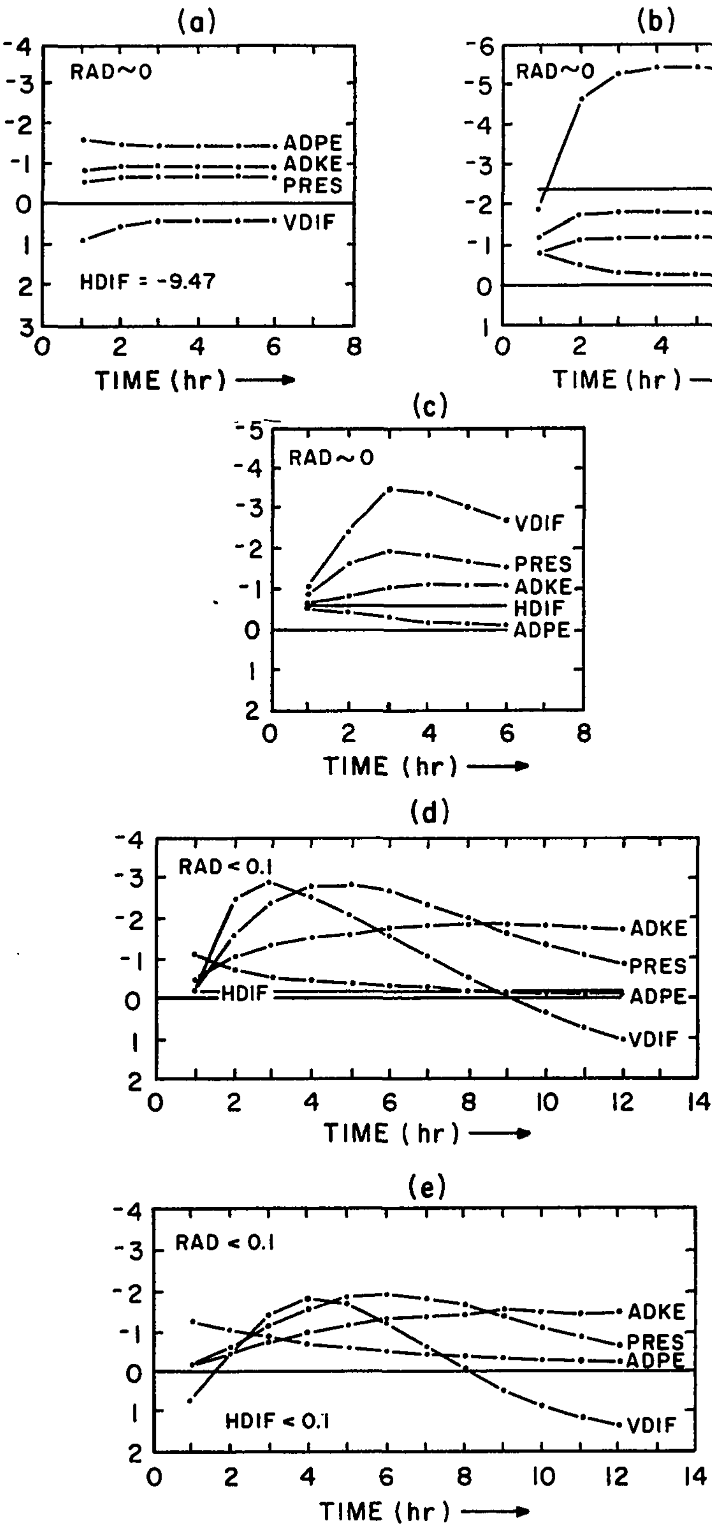

Fig. 11. Sources and sinks of total energy for subsidence cases expressed as a fraction of the total energy: a) 5 km, b) 10 km, c) 20 km, d) 50 km, and e) 100 km. Negative values indicate sinks. See text for explanation of abbreviations.

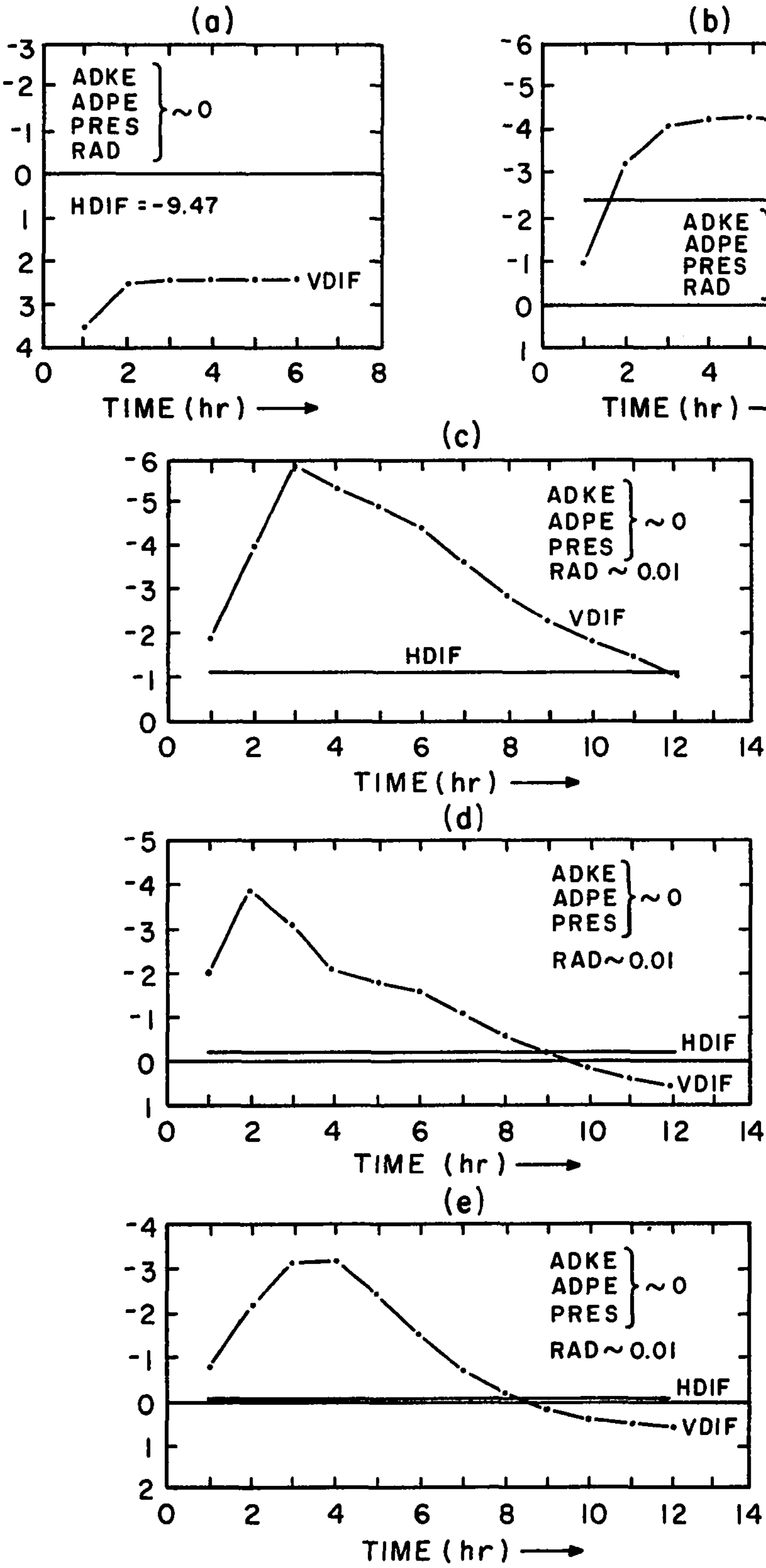

Fig. 12. Sources and sinks of total energy for non-subsidence cases. See Fig. 11.

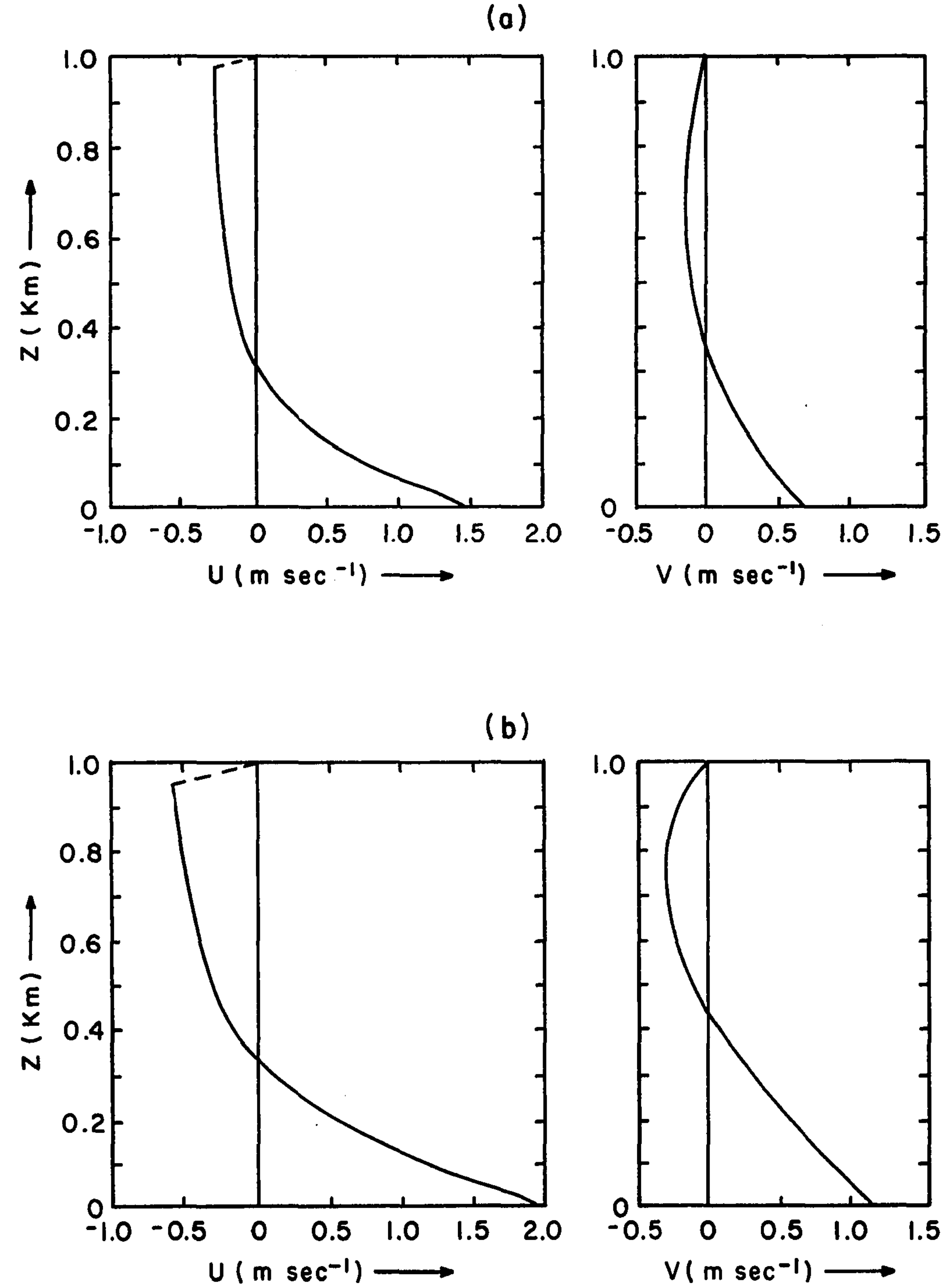

Fig. 13. Horizontal velocities U and V as a function of height for 50-km cases at t = 3 hr: a) subsidence case; b) non-subsidence case.

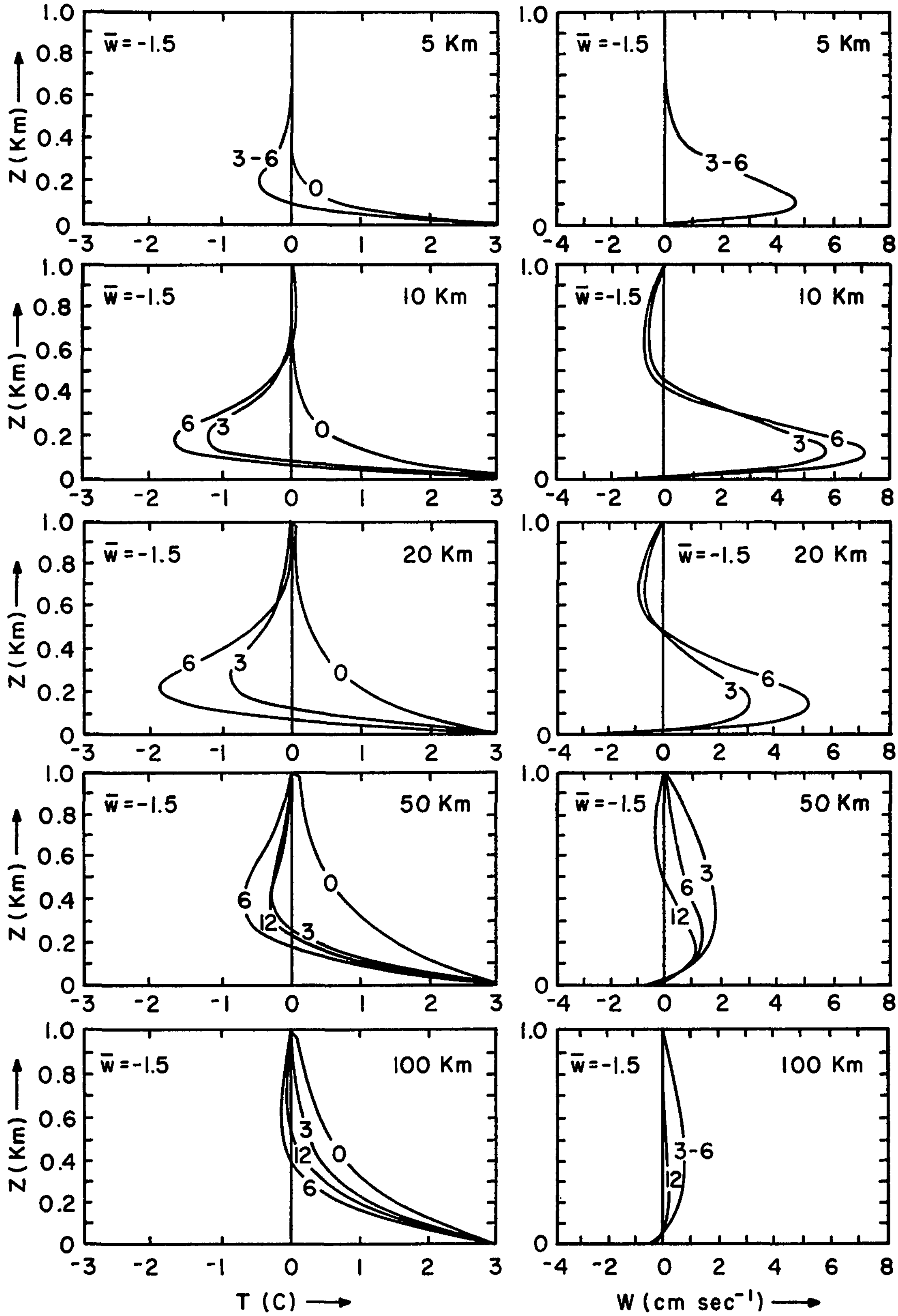

Fig. 14. Excess temperature and vertical motion as a function of height for subsidence cases at selected times indicated by the number on the curves (in hours).

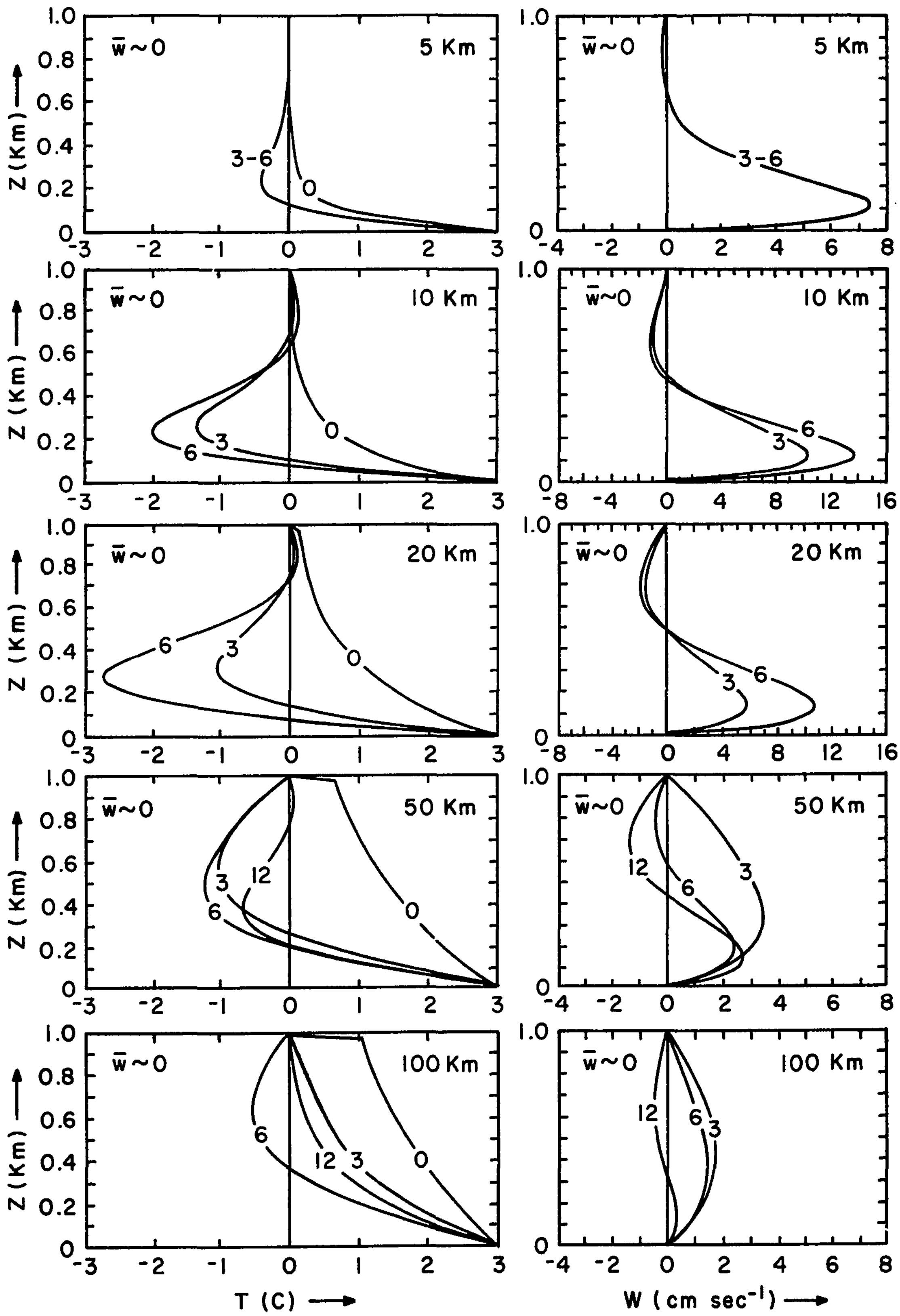

Fig. 15. Same as Fig. 14, but for non-subsidence cases. Note change in scale of W in the 10- and 20-km cases.

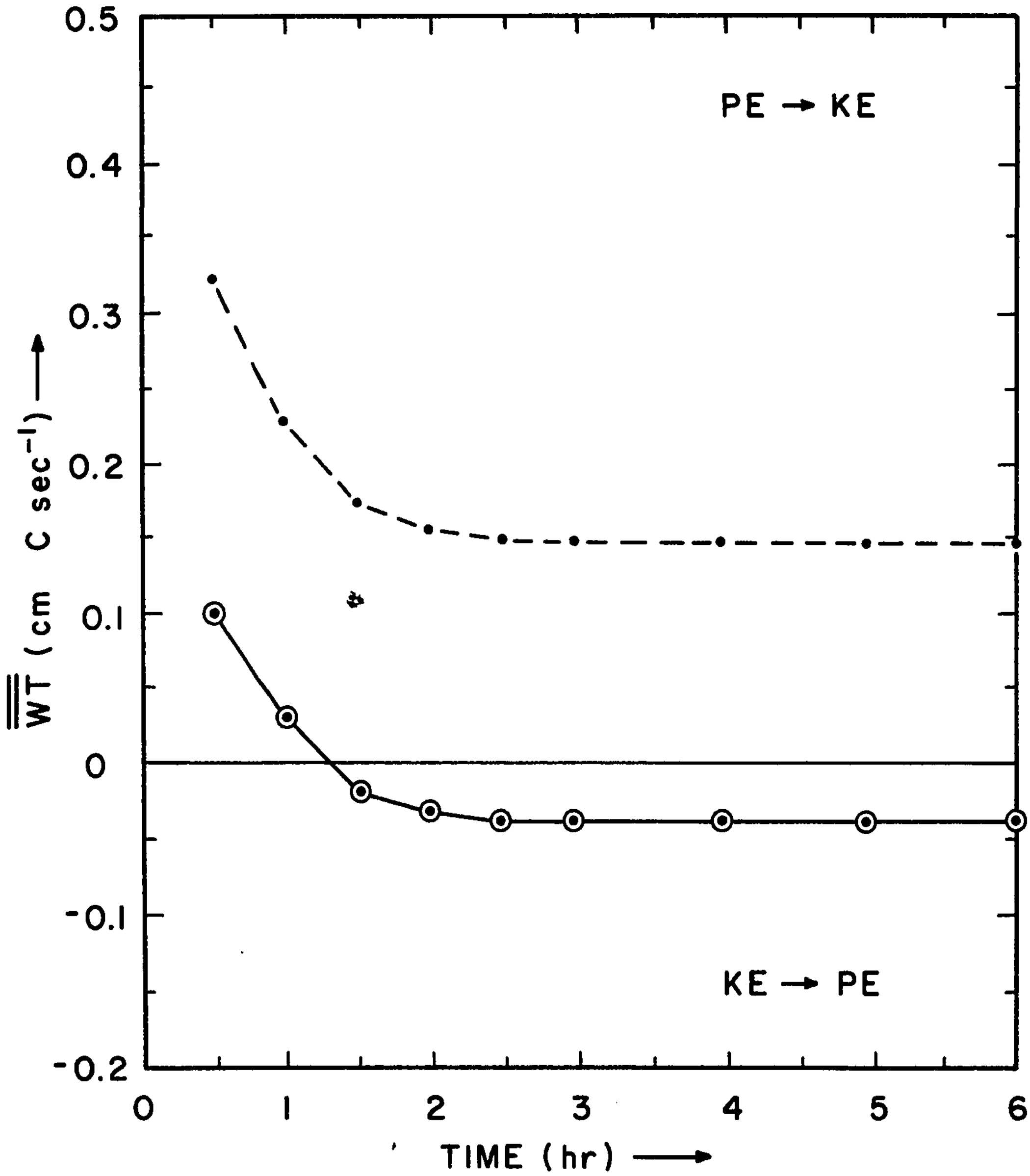

Fig. 16. Vertically-averaged convective heat transport for the 5-km cases. See Fig. 10 for explanation.

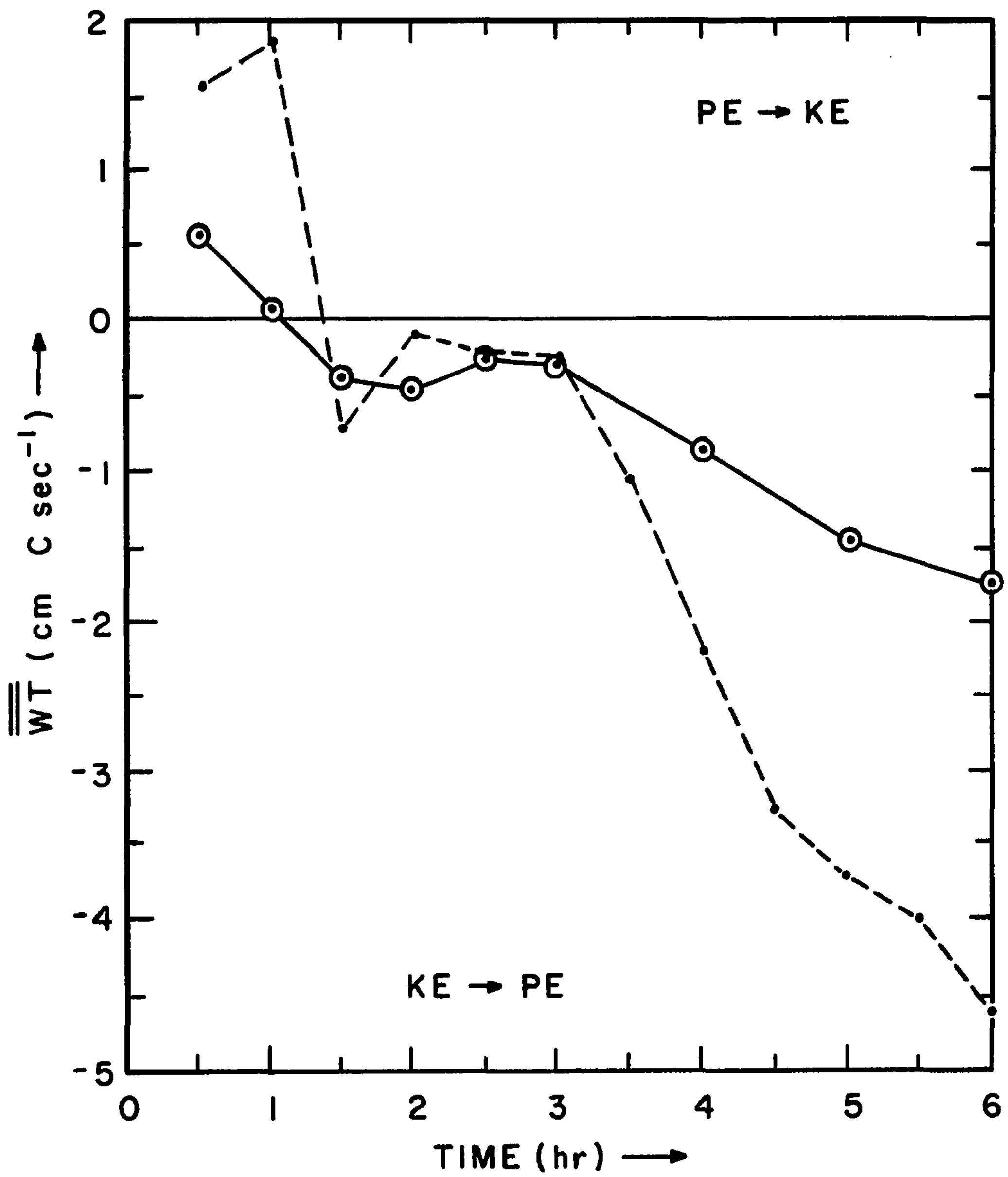

Fig. 17. Vertically-averaged convective heat transport for the 20-km cases. See Fig. 10 for explanation.

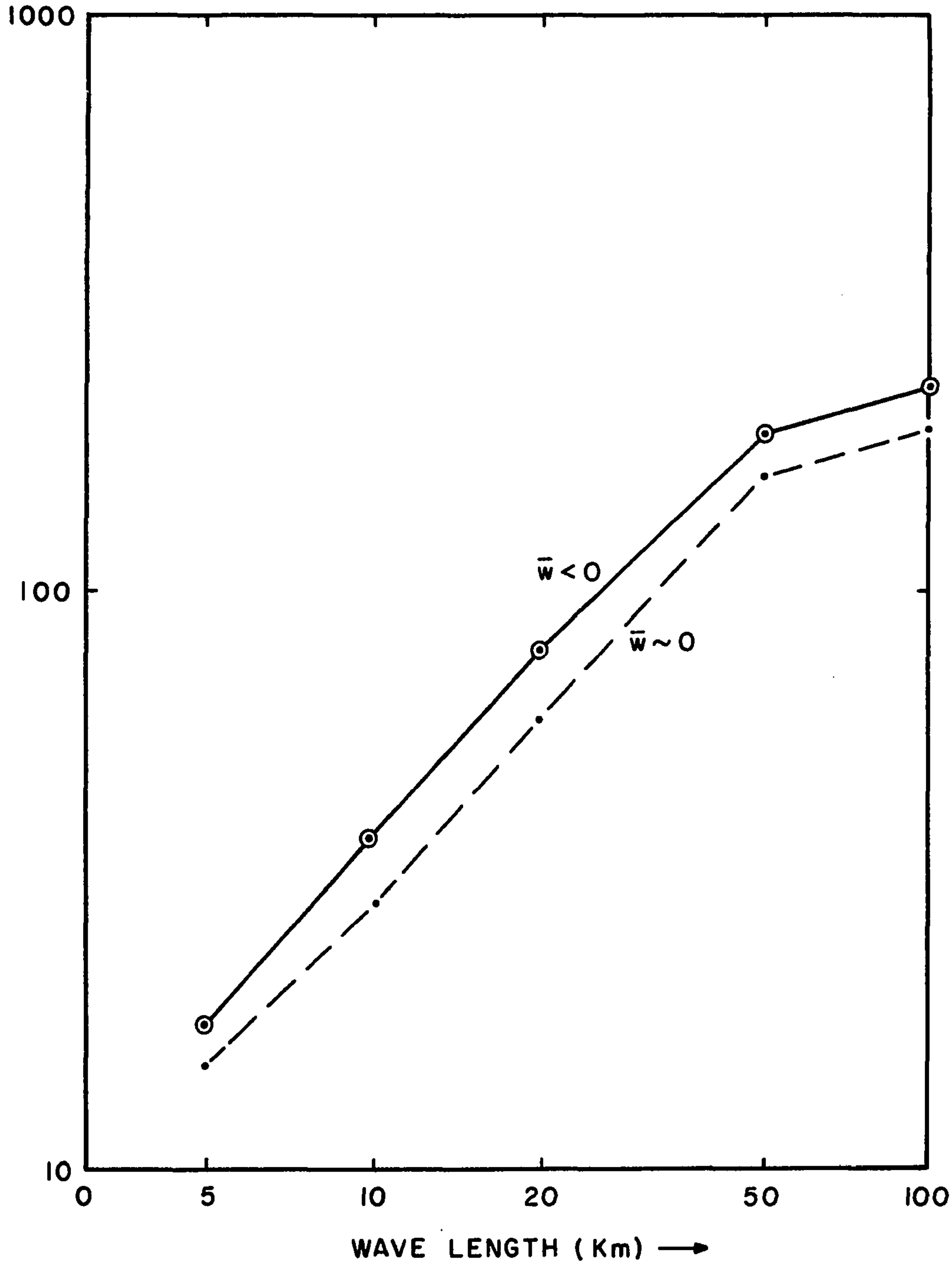

Fig. 18. Ratio of horizontal to vertical velocity maxima at t = 6 hr for subsidence and non-subsidence cases.

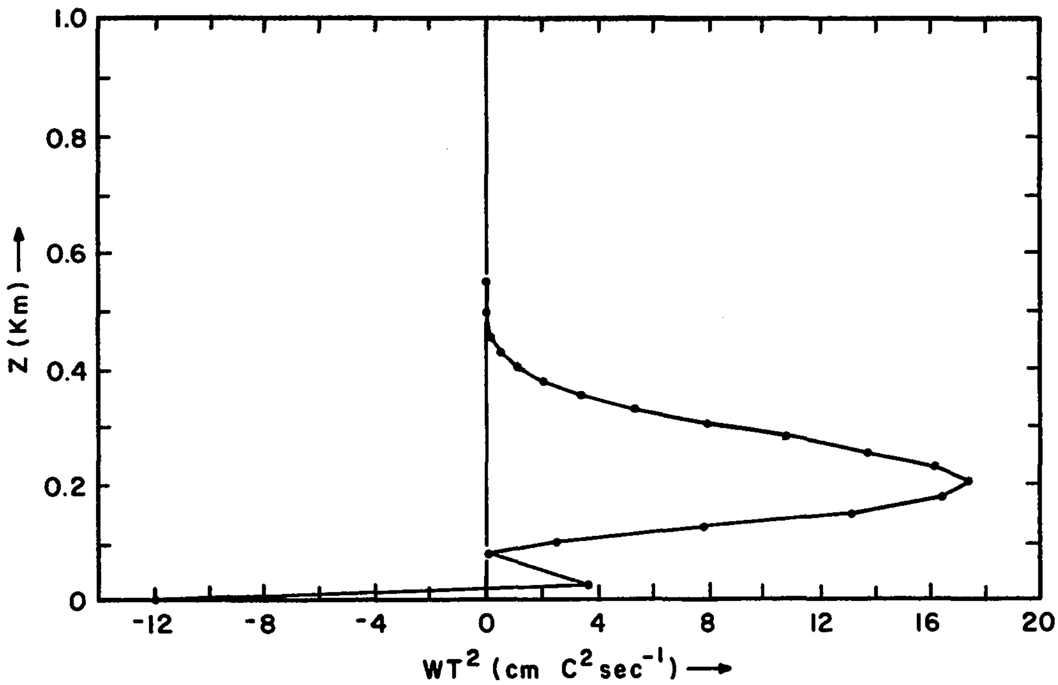

Fig. 19. Vertical distribution of WT^2 at t = 6 hr for the 20-km subsidence case.

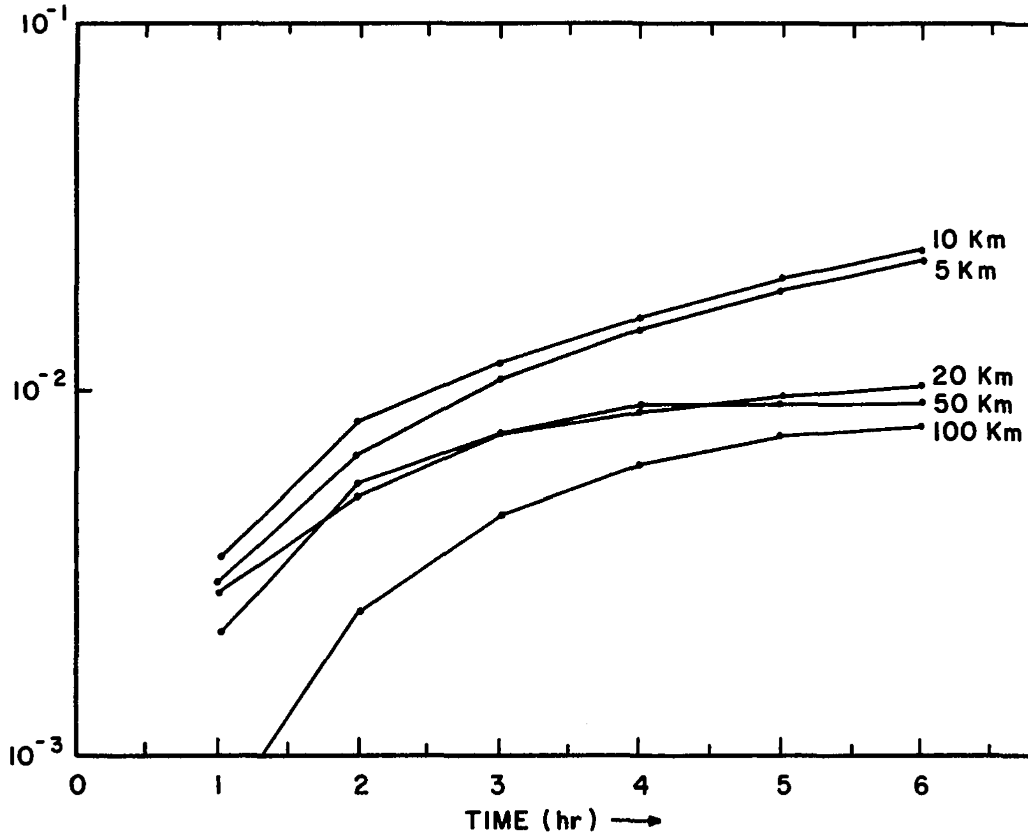

Fig. 20. Ratio of cumulative error in evaluation of total energy integral to total energy for subsidence cases.

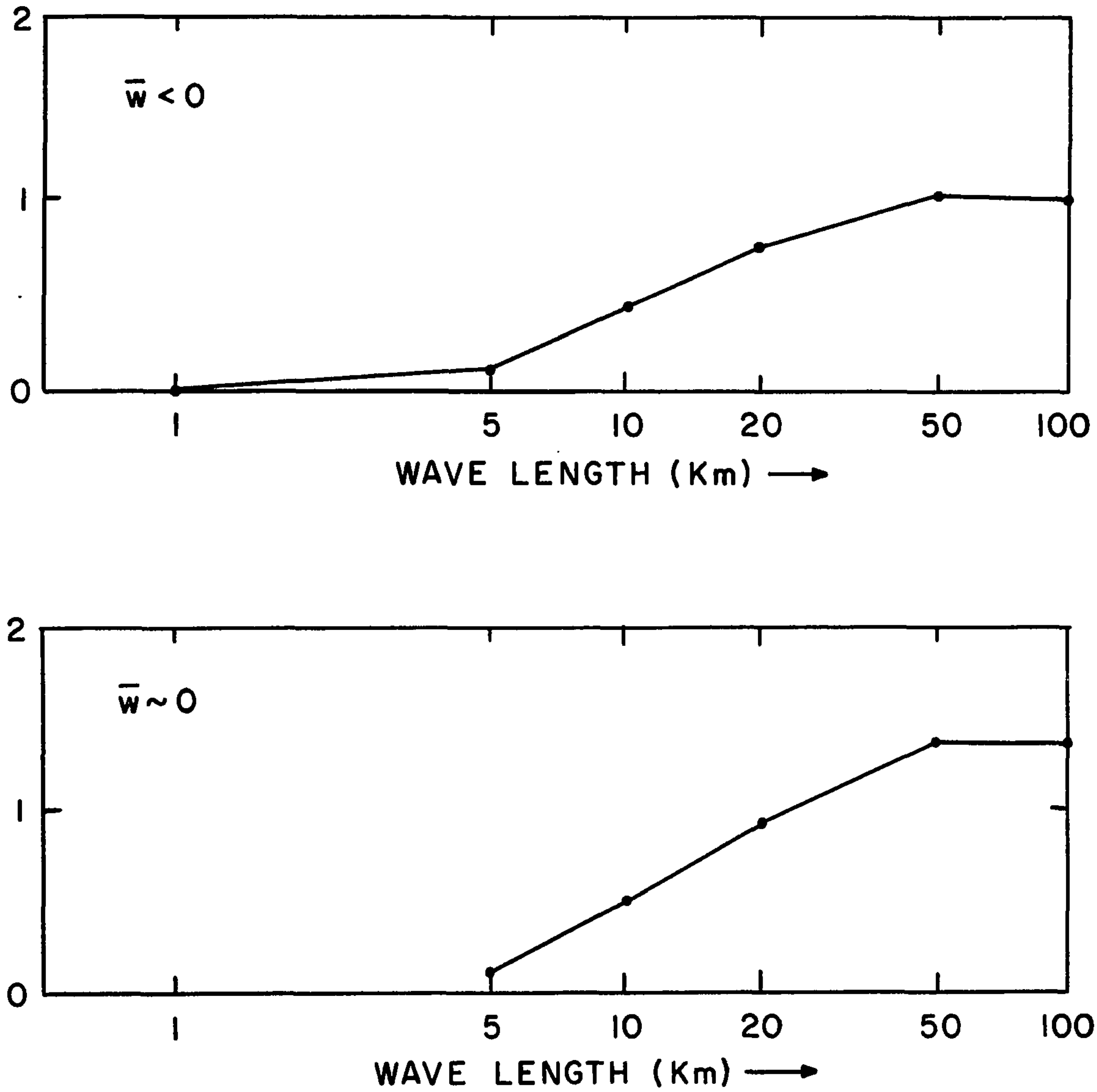

Fig. 21. Effect of Coriolis for subsidence and non-subsidence cases. Curves show ratio $|v_{max}| / |u_{max}|$ at t = 6 hr.

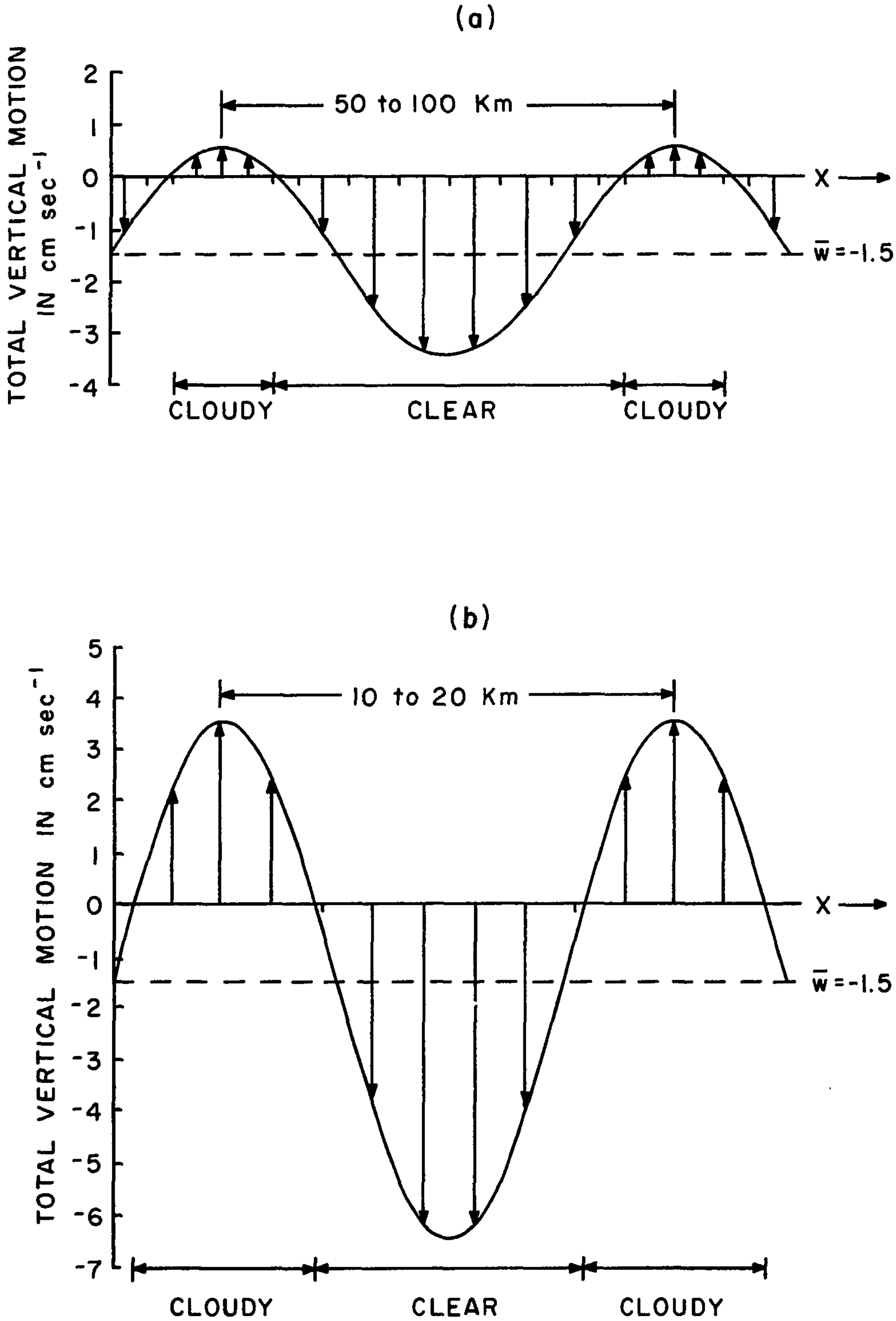

Fig. 22. Subsidence effect on ratio of cloudy to clear air in small-scale (10 to 20 km) and large-scale (50 to 100 km) perturbations.